Geochimica et Cosmochimica Acta 383 (2024) 1–17

Contents lists available at ScienceDirect

Geochimica et Cosmochimica Acta

journal homepage: www.elsevier.com/locate/gca

Potassium isotope compositions of Mariana arc lavas and their sedimentary input

Joel B. Rodney [a,*], Théo Tacail [a,b], Jamie Lewis [a], Morten B. Andersen [c], Tim Elliott [a]

[a] Bristol Isotope Group, School of Earth Sciences, University of Bristol, Wills Memorial Building, Queen's Road, Bristol BS8 1RJ, UK
[b] Institute of Geosciences, Johannes Gutenberg University, Mainz, Germany
[c] School of Earth & Environmental Sciences, Cardiff University, Park Place, Cardiff CF10 3AT, UK

ARTICLE INFO

Associate editor: Fangzhen Teng

Keywords:
Potassium isotopes
Mariana arc
Subduction
Slab dehydration
Sediment melt

ABSTRACT

We apply the stable potassium isotope system ($^{41}K/^{39}K$) to well-studied Mariana arc lavas, in which inter-island geochemical variability has been interpreted to reflect near constant addition of an aqueous fluid flux, that dominantly samples the subducting mafic oceanic crust and variable amounts of sediment melt addition to the sub-arc mantle wedge. The nature of the sediment component in the Mariana arc lavas remains enigmatic, with a mixture of melts from all subducted sediment lithologies and the altered-mafic oceanic crust seeming likely, but some interpretations point towards a component from melting of the volcaniclastic sediment alone. We present K isotopic data on a set of well-characterised Mariana arc lavas and sediment samples (from Ocean Drilling Program site 801). Our data show that the majority of Mariana arc lavas are isotopically heavy ($\delta^{41}K$), by up to ~0.2 ‰, relative to mid-ocean ridge basalt (MORB), but most of the subducting sediment samples are slightly isotopically lighter than, or indistinguishable from MORB. The volumetrically important volcaniclastic sedimentary unit however is significantly isotopically lighter than MORB, by ~0.8 ‰, which reflects marine diagenetic processes. Thus, volcaniclastic material significantly influences the bulk sediment K isotope composition. We show that $\delta^{41}K$ compositions of the Mariana arc lavas can be reproduced by the addition of an aqueous fluid with isotopically heavy K (relative to MORB) and an additional fraction of an incompatible-element-enriched isotopically light melt component. Modelling of K isotopes together with K/La and radiogenic Nd indicate that the melt component is best explained by a mix of melts from bulk sediment and altered-mafic oceanic crust. Our results show that distinctive K isotopic variations in subduction zone inputs and K isotopic fractionation during dehydration reactions makes K a useful tracer of subduction zone processes.

1. Introduction

Volcanic arc lavas show distinct patterns in trace element ratios and radiogenic isotopic compositions that can be reconciled with the addition of elements from various subducting components to the overlying mantle wedge (e.g., Pearce, 1983; Hawkesworth et al., 1993). However, the exact nature of these components (e.g., aqueous fluid, sediment derived fluid, sediment melt, altered-mafic oceanic crust melt or mélange mix and melt) is debated and may vary between arcs (e.g., Elliott et al., 1997; Marschall and Schumacher, 2012; Nielsen and Marschall, 2017; Turner and Langmuir, 2022). Novel stable isotope systems offer new ways to trace processes that occur during subduction, as well as distinguishing between types of slab derived components added to the sub-arc mantle wedge (e.g., Prytulak et al., 2013; Andersen et al., 2015; Freymuth et al., 2015; Debret et al., 2016; König et al., 2016; Pons et al., 2016; Klaver et al., 2020; Mazza et al., 2020; Nielsen et al., 2020; Wu et al., 2020; Hu et al., 2021a; Chen et al., 2022; Parendo et al., 2022b; Stubbs et al., 2022).

Arc lavas are enriched in heavy alkali and alkaline earth elements (e.g., K, Rb, Cs, and Ba) and some other, highly incompatible, elements (e.g., Mo, W, Pb, and U) all of which are interpreted to be mobile in aqueous fluids released during the dehydration of subducting slabs (König et al., 2016; Chen et al., 2019b; Freymuth et al., 2019; Mazza et al., 2020; Stubbs et al., 2022). This enrichment is marked when compared to elements of similar incompatibility during mantle melting, which are 'fluid immobile', such as Th, La, and Nb, resulting in

* Corresponding author.
E-mail addresses: joel.rodney@bristol.ac.uk (J.B. Rodney), theo.tacail@protonmail.com (T. Tacail), jamie.lewis@bristol.ac.uk (J. Lewis), andersenm1@cardiff.ac.uk (M.B. Andersen), tim.elliott@bristol.ac.uk (T. Elliott).

https://doi.org/10.1016/j.gca.2024.07.035
Received 3 January 2024; Accepted 29 July 2024
Available online 2 August 2024

distinctive trace element ratios, e.g., elevated Ba/Th in arc lavas (e.g., Elliott, 2003). Other sources of incompatible element enrichments in arc lavas are subducted sediments that potentially influence the composition of the sub-arc mantle wedge through fluids released during dehydration or melting (e.g., Plank and Langmuir, 1993). The stable isotope systematics of elements enriched in arc lavas offer a promising way to investigate processes occurring during subduction. One such emerging stable isotope system is K (e.g., Li et al., 2016; Wang and Jacobsen, 2016; Chen et al., 2019a; Tuller-Ross et al., 2019b; Hu et al., 2020; Liu et al., 2020; Santiago Ramos et al., 2020; Wang et al., 2020; Parendo et al., 2022a, 2022b).

There are significant elemental enrichments in K and notable isotopic variations (reported in permille, ‰ as δ^{41}K, the ^{41}K/^{39}K ratio relative to reference material NIST SRM3141a; $\delta^{41}K = [(^{41}K/^{39}K)_{sample}/(^{41}K/^{39}K)_{NIST\ SRM3141a} - 1]$) in subducting components relative to the composition of the upper mantle as defined by mid-ocean ridge basalt (MORB) (Tuller-Ross et al., 2019b) (Fig. 1). This large variability in the K isotope system in subduction zone inputs suggests that K has potential to trace processes of subduction (Fig. 1).

Studies on the Lesser Antilles and Izu arcs have shown K isotopic variability in their lavas and compositions distinct from the upper mantle as represented by MORB (Hu et al., 2021a; Parendo et al., 2022b) (Fig. 1). Values of δ^{41}K in arc lavas higher than MORB have been proposed to reflect the addition, to the mantle source, of an aqueous fluid released during subducting slab dehydration. It is inferred that K isotope compositions are fractionated by the preference of lighter K isotopes, for retained solid phases such as phengite, in the subducting crust (Liu et al., 2020; Parendo et al., 2022b). Wang and Ionov (2023) report K isotopic data on a set of sub-arc mantle harzburgite xenoliths that have undergone metasomatism by subduction zone fluids that span a broad range in δ^{41}K and commonly show enrichment in heavy K isotopes (Fig. 1). This sense of fractionation is also re-affirmed from the composition of a set of exhumed eclogites, which represent the residue of dehydrated subducted mafic crust; these data extend to extremely low δ^{41}K values explainable by the loss of isotopically heavy K to aqueous fluids released from the subducting slab (Liu et al., 2020) (Fig. 1). However, some arc lavas have δ^{41}K lower than MORB, notably in the Lesser Antilles arc, and this is thought to reflect the addition of small amounts (<1 to 5 %) of sediment melts to their mantle sources (Hu et al., 2021a) (Fig. 1). Given the variability in subducting components, individual arc settings need to be investigated on a case-by-case basis to test the potential of K isotopes as a tracer of slab components added to the sources of arcs lavas.

Here we apply the K isotopic system to a set of well-studied Mariana arc lava samples and associated subducting sediments (Elliott et al., 1997), and examine models that re-produce Mariana arc lavas using subducting slab derived components. Mariana arc lavas show inter-island geochemical variations that have been argued to reflect the variable addition of a sediment component and near constant addition of an aqueous fluid component to their mantle source (Elliott et al., 1997). The subducting sediment pile outboard of the Mariana arc is composed of distinct sedimentological units that can be grouped into pelagic clays, chert and porcellanite, volcaniclastics, and radiolarite and claystones. The units have contrasting chemical compositions that help identify their possible contributions to the Mariana arc lava sources (Elliott et al., 1997; Plank and Langmuir, 1998).

Previously, radiogenic isotope compositions (e.g., Sr, Nd, and Pb) have been a major tool used to distinguish between the different components in the Mariana arc lava source (e.g., Meijer, 1976; Woodhead and Fraser, 1985; Woodhead, 1989; Elliott et al., 1997; Tollstrup and Gill, 2005; Avanzinelli et al., 2012; Freymuth et al., 2015). Unradiogenic Pb compositions in the Mariana arc lavas represent a sediment-poor, aqueous fluid signature, while more radiogenic Pb compositions project towards enriched sediment components (Fig. 2).

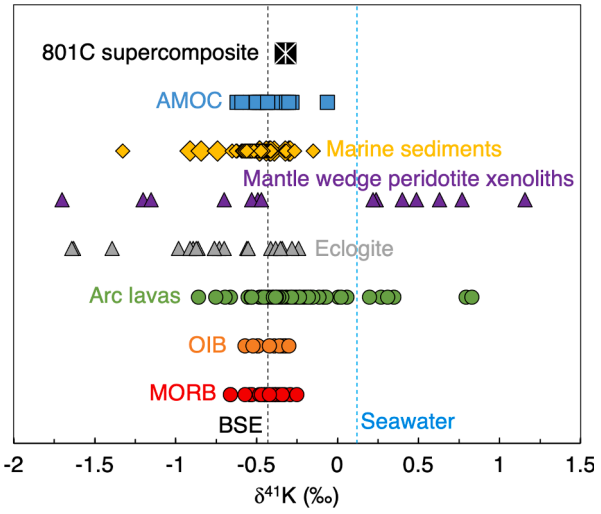

Fig. 1. Plot of K isotopic compositions of MORB, ocean island basalts (OIB), arc lavas, eclogite, peridotite, marine sediments, and AMOC. Modern seawater composition is from Wang et al. (2020) and is shown as a vertical dashed blue line. The bulk silicate Earth composition (BSE) is from Tuller-Ross et al. (2019b) and is shown as a vertical dashed black line. Mid-ocean ridge basalt and OIB data are from Tuller-Ross et al. (2019b). Arc lava data are from Hu et al. (2021a) and Parendo et al. (2022b). Eclogite data are from Liu et al. (2020) and mantle wedge peridotite xenolith data are from Wang and Ionov (2023). Marine sediment data includes average of several global sediment columns from Hu et al. (2020) and are plotted as the larger yellow diamonds along with other marine sediment data from Parendo et al. (2022a). Altered-mafic oceanic crust data and the 801C supercomposite is from Hu et al. (2020). The 801C supercomposite AMOC sample is made from lithological components of AMOC mixed in proportion to their abundance to represent average AMOC (Kelley et al., 2003).

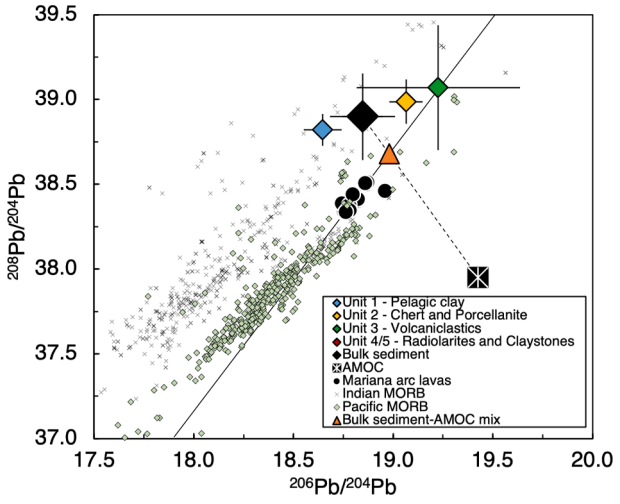

Fig. 2. A regression line (solid line) for the Mariana arc lavas, from the volcanic islands in the Mariana central island province, in a plot of ^{208}Pb/^{204}Pb vs. ^{206}Pb/^{204}Pb. Stippled line between bulk sediment and AMOC is calculated as the mixture that intersects the Mariana arc lava regression line and is shown as an orange triangle. The average mixing proportion for the mass fraction of Pb from bulk sediment is 77 % and 23 % from AMOC, and accounting for uncertainty in the bulk sediment composition, this corresponds to mixing proportions of ~90 to 60 % Pb from bulk sediment. Converting this to a mass fraction of bulk materials, given Pb concentrations in bulk sediment and AMOC, this is equal to an average of ~18 % bulk sediment and ~82 % bulk AMOC by mass. Given uncertainties this results in a range of between 37 to 9 % bulk sediment and 63 to 91 % bulk AMOC by mass. Also shown are Pacific MORB (green diamonds), Indian MORB (crosses) (Stracke, 2012 supplementary table 1), ODP 801 sediment units (diamonds) and AMOC (starred square) (Freymuth et al., 2015). Unit 4/5 plots in the same position as the bulk sediment. The figure is re-created and modified from Freymuth et al. (2015).

The Mariana arc lavas form an array in $^{208}Pb/^{204}Pb$ against $^{206}Pb/^{204}Pb$, with a best fit line that back-projects through a Pacific MORB end-member (Freymuth et al., 2015) (Fig. 2). The unaltered, subducting mafic oceanic crust at the Mariana arc has a typical Pacific MORB composition, while the sub-arc mantle below the Mariana arc has a typical Indian MORB isotopic composition (Pearce et al., 1999). The Pb, and by inference the K, in the Mariana arc lavas is therefore dominantly sourced from the unaltered subducting crust. Lead isotopic systematics are inconsistent with a fluid component coming from the most altered upper part of oceanic crust (Avanzinelli et al., 2012). The source of fluid in a component that dominantly samples Pb from the deeper unaltered mafic crust is likely from dehydration of the underlying subducted serpentinitised mantle (e.g., Ulmer and Trommsdorff, 1995; Deschamps et al., 2013; Spandler and Pirard, 2013). This also satisfies constraints from redox sensitive elements such as Mo, U, and W measured in the Mariana arc lavas and other eclogites, that make a case for oxidising slab fluids derived from serpentinite dehydration (e.g., Andersen et al., 2015; Chen et al., 2019b; Stubbs et al., 2022).

One aspect of Mariana arc lava studies that has remained unresolved is the composition of the sediment component. Pelagic clays and volcaniclastic lithologies dominate the sedimentary budgets of incompatible trace elements (Elliott et al., 1997) but are chemically very distinct from one another (Plank and Langmuir, 1998). Previous studies have suggested either a dominant volcaniclastic component (e.g., Tollstrup and Gill, 2005; Avanzinelli et al., 2012; Martindale et al., 2013) or a mix of bulk sediment (all sediment lithologies averaged) and altered-mafic oceanic crust (AMOC) (e.g., Freymuth et al., 2015). On the array of $^{208}Pb/^{204}Pb$ against $^{206}Pb/^{204}Pb$ subducting sediments plot at the radiogenic end of the array (Fig. 2). Volcaniclastic sediments are the most radiogenic in $^{208}Pb/^{204}Pb$ and $^{206}Pb/^{204}Pb$ and fall on the trend line defined by the Mariana arc lavas, indicating their potential as a sedimentary component in the arc lava source (Fig. 2), while pelagic clays, chert and porcellanite, radiolarite and claystones, and a bulk sediment mix are too un-radiogenic in $^{206}Pb/^{204}Pb$ to form an appropriate endmember for the Pb isotope mixing array (Fig. 2). However, a mix of the bulk sediment component with AMOC (with radiogenic $^{206}Pb/^{204}Pb$), could fall on the trend line and would fit as an enriched, radiogenic Pb isotope end member composition (Fig. 2). Given the large isotopic variations found between some sediments and AMOC (Hu et al., 2020) (Fig. 1), K isotopes may offer a unique perspective on this debate and aid in narrowing the composition of the sediment component added to the Mariana sub-arc mantle.

2. Geological settings and sample description

2.1. The Mariana arc

The Mariana volcanic arc, located in the western Pacific Ocean, forms the southern portion of the Izu-Bonin-Mariana subduction zone that stretches 2500 km and has been active since ~45 Ma (Meijer et al., 1983) (Fig. 3). Jurassic to Cretaceous aged Pacific oceanic crust, with overlying sediment cover, subducts westwards beneath the Philippine sea plate at ~4 cm yr^{-1} (Seno, 1977; Stern et al., 2003). As an intra-oceanic convergent margin, the potential impact of continental crust contamination on arc lavas is minimised (Stern et al., 2003). There is no observable accretionary prism (von Huene and Scholl, 1991), suggesting that a large majority of the sediment package is subducted, allowing studies of outboard sediments to characterise subduction zone inputs.

The Mariana arc system is split into the southern seamount, central island and northern seamount provinces (Bloomer et al., 1989); the samples in this study come from the central island province. The samples, originally described in Elliott et al. (1997), have been well characterised for their trace element, radiogenic, and stable isotope compositions (Elliott et al., 1997; Avanzinelli et al., 2012; Prytulak et al., 2013; Andersen et al., 2015; Freymuth et al., 2015; Klaver et al., 2020; Stubbs et al., 2022). They are Holocene-age lavas with minimal impact from recent alteration.

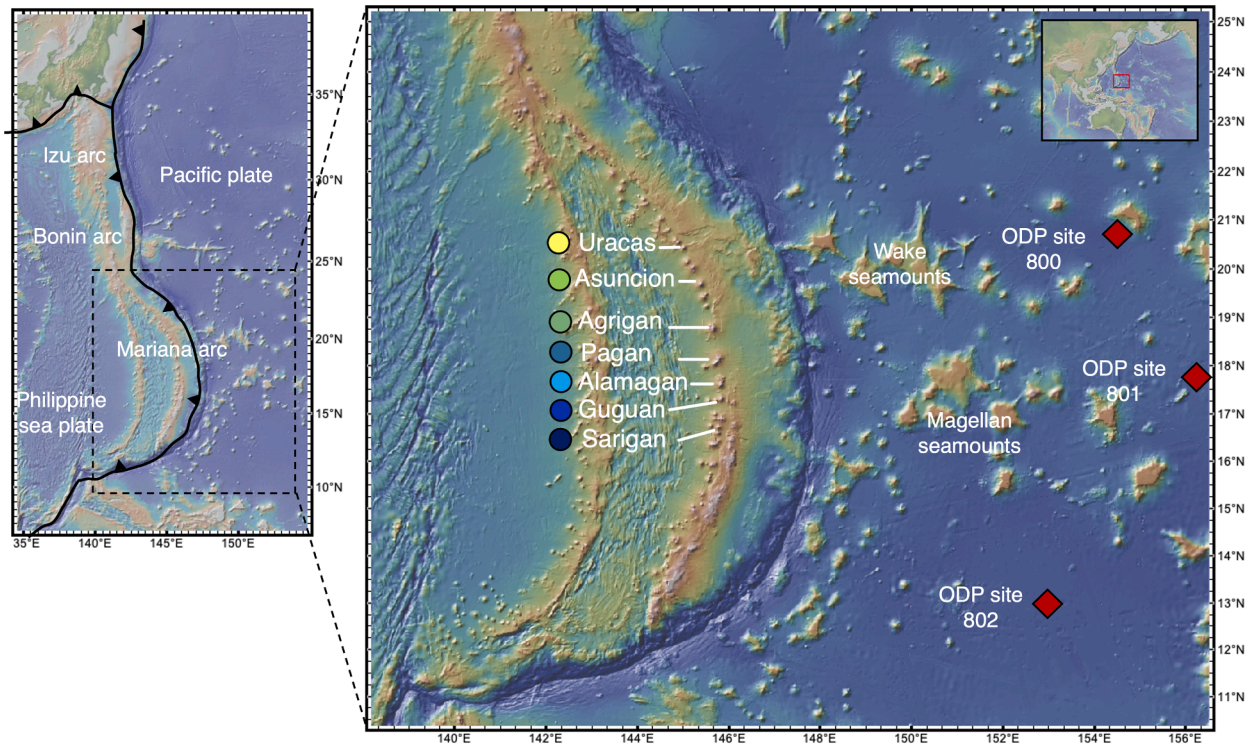

Fig. 3. Map of the Izu-Bonin-Mariana arc and a smaller scale map of the Mariana arc showing the location of the islands of central island province and locations of the ocean drilling programme (ODP) sites 800, 801, and 802. Base map from Geomapapp (http://www.geomapapp.org).

2.2. Mariana arc lavas

The central island province of the Mariana islands comprises a number of volcanic islands that erupt basalt to basaltic andesite composition lavas (Meijer, 1976; Dixon and Batiza, 1979; Hellman et al., 1979; Stern, 1979; Chow et al., 1980; Meijer and Reagan, 1981; Stern and Ito, 1983; Hole et al., 1984; White and Patchett, 1984; Woodhead and Fraser, 1985; Ito and Stern, 1986; Woodhead, 1988, 1989; Elliott et al., 1997; Pearce et al., 1999; Elliott, 2003; Ito et al., 2003; Stern et al., 2003; Pallister et al., 2005; Pearce et al., 2005; Tollstrup and Gill, 2005; Wade et al., 2005; Stern et al., 2006; Kelley et al., 2010; Marske et al., 2011; Woodhead et al., 2011; Avanzinelli et al., 2012; Kelley and Cottrell, 2012; Prytulak et al., 2013; Tamura et al., 2014; Andersen et al., 2015; Freymuth et al., 2015; Ikeda et al., 2016; Williams et al., 2018; Klaver et al., 2020; Stubbs et al., 2022). The initial mantle source of the Mariana arc lavas is inferred to be more chemically depleted than the average MORB source (Woodhead et al., 1993) and the addition of any incompatible elements to the mantle source should have a large control on the resulting geochemical and isotopic characteristics of the arc lavas.

We measured samples from each of the following islands: Guguan (GUG3, GUG6, GUG9, GUG11, and GUG12), Pagan (PAG1 and PAG3), Agrigan (AGR2, AGR4b, AGR5, and MM-92-6), Asuncion (ASC3ba), and Uracas (URA5, URA7, and URA12). These islands cover the full range of compositional variability identified in Elliott et al. (1997) (Fig. 4). Lavas from Guguan are the most incompatible element depleted, with high K/Th and low $(La/Sm)_N$ reflecting the dominance of a fluid component (Fig. 4). Lavas from Agrigan and Uracas show opposite characteristics in these ratios reflecting the addition of a (low K/Th) sediment component that overprints the fluid addition (Fig. 4) (Elliott et al., 1997). The Asuncion and Pagan samples have intermediate compositions between these extremes, albeit with Pagan being more similar to the depleted Guguan samples. These samples allow us to investigate if the addition of variable amounts of slab components is reflected in the K isotopic composition of the Mariana arc lavas. Note that sample PAG1 has a limited selection of trace element data available and for the purpose of this study we report K isotopic data for the sample, but do not include it in certain figures and our discussion.

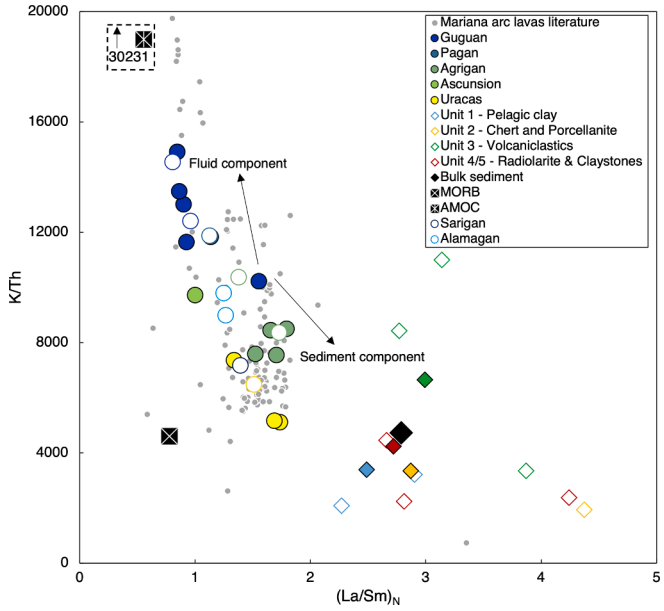

Fig. 4. Plot of K/Th ratio against chondrite normalised La/Sm ratio for Mariana arc central island province lavas and sediments from ODP site 801. Mariana arc lava samples shown as large circles are those from Elliott et al. (1997), filled circle symbols are those used in this study and hollow samples those not used in this study. Sediments are shown as diamonds, filled diamonds represent average unit compositions and hollow samples the discrete samples measured. Estimates of mean MORB and AMOC compositions are from Gale et al. (2013) and Kelley et al. (2003) respectively, where the AMOC sample represents the supercomposite of AMOC at ODP site 801C. Note that the AMOC composition plots off the y-axis scale and the K/Th ratio is indicated in the dashed box. Small grey circles are literature data for the central island province (Dixon and Batiza, 1979; Hellman et al., 1979; Hole et al., 1984; Pearce et al., 1999; Pallister et al., 2005; Wade et al., 2005; Stern et al., 2006; Kelley et al., 2010; Marske et al., 2011; Woodhead et al., 2011; Kelley and Cottrell, 2012; Tamura et al., 2014; Ikeda et al., 2016).

2.3. Mariana arc sediments

There have been several Ocean Drilling Program (ODP) cores made of the sediment package and magmatic oceanic crust located to the east of the subduction zone, most notably those from ODP leg 129 drill sites (holes 800, 801, and 802) located ~500 to 700 km east of the Mariana trench (Fig. 3). These drill holes penetrate the entire sediment package and sample the full range of sedimentary lithologies, allowing an investigation of the potential sediments that have subducted below the Mariana arc (Salimullah and Stow, 1992). The AMOC section of site 801 is represented by 417 m of 170 Ma magmatic oceanic crust, allowing for the characterisation of the AMOC that subducts at the Mariana trench (e.g., Hauff et al., 2003; Kelley et al., 2003; Andersen et al., 2015; Freymuth et al., 2015; Hu et al., 2020).

We have measured the K isotope ratios in sediment samples from ODP site 801 from the distinct sedimentological units (Fig. 4). These units are 65 m of Cenozoic clay (Unit 1 – Pelagic Clay, two samples), 60 m of Late Cretaceous chert and porcellanite (Unit 2 – Chert and Porcellanite, one sample), 190 m of Early Cretaceous volcaniclastic turbidities (Unit 3 – Volcaniclastics, three samples), and 140 m of Jurassic radiolarite and claystones (Unit 4/5 – Radiolarite and Claystone, three samples) (Lancelot et al., 1990). The thickness of the sediment units is variable between sites 800, 801, and 802 but overall volcaniclastic sediments are dominant volumetrically, ~55 % at each site.

Average unit compositions can be proportioned according to sediment thickness and density, following Plank and Langmuir (1998) to form a bulk sediment composition that represents the average subducting sediment composition (Fig. 4). Our individual sediment samples are originally from the study of Freymuth et al. (2015) and were sampled in near identical positions in sediment cores to original samples from Karpoff (1992) and Plank and Langmuir (1998), with updated major and trace element data from Vervoort et al. (2011); this is apart from sample 801B-7R1-34 which is from Karpoff (1992) and Plank and Langmuir (1998). Major, trace element and radiogenic isotopic data for average sediment unit compositions and the bulk sediment composition are from Elliott et al. (1997).

3. Analytical methods

3.1. Separation techniques for stable K isotopic analysis

Approximately 50 mg of whole rock Mariana arc lava powders and ODP site 801 sediments were digested in a 5:1 vol ratio of 4 ml concentrated HNO_3 and 0.8 ml concentrated HF acid mixture in clean PFA beakers on a hot plate at 120 °C for two days. Samples were then evaporated to dryness and re-dissolved twice in 6 M HCl to remove fluoride precipitates and achieve full sample dissolution. Samples were then re-dissolved in 1 M HNO_3 for column chemistry. A two-column method following Tacail et al. (2023) was used for K separation with a third column following Wu et al. (2016) used for the separation of V from K. We have found that the initial two stages do not effectively separate V from K and that V biases K isotope ratio measurements at V/K ratios common in basaltic rocks (Fig. S1, Table S1, see Supplementary Material for details).

Aliquots of samples containing approximately 10–100 μg of K were

processed through ion exchange purification. Samples were initially loaded in 1 ml 1 M HNO_3 onto 2.5 ml BioRad AG50W-X12 200–400 mesh cation exchange resin in PFA columns with a 7.5 mm internal diameter. A 0.5 M HF solution was used to elute Fe, Al, and U before the elution of most of the matrix using 1 M HNO_3, with K fractions collected between the elution of Na and Rb. Collected K fractions were re-dissolved in 0.25 ml 0.4 M HCl and loaded onto PTFE shrink fit columns (with a 4 mm internal diameter) with 0.25 ml BioRad AG50W-X12 200–400 mesh cation exchange resin for the removal of residual matrix elements (Na and Mg). Collected K fractions were re-dissolved in 0.5 ml of a 0.01 M HCl – 1 % H_2O_2 mixture and loaded onto BioRad Poly-Prep columns with 0.5 ml AG1-X8 200–400 mesh anionic exchange resin. Vanadium is retained on the resin and K was eluted with 10 ml 0.01 M HCl – 1 % H_2O_2. After each column step collected K fractions were fluxed in 1 ml 1:1 vol ratio of concentrated HNO_3: 30 % H_2O_2 mixture to remove any organic material that may have eluted off the resins. Samples were re-dissolved in ~0.3 M HNO_3 and further diluted to 1 ug g^{-1} K concentration for isotopic analysis. Potassium recovery was over 99.5 % and monitored by the collection and measurement of 'split fractions' pre and post the K elution window, to ensure they contained negligible K. This procedure guards against chromatography induced, mass-dependent isotope fractionation in the collected K aliquot.

Our chemical purification methods resulted in major and trace element/K ratios typically below 0.00001–0.01 (Tacail et al., 2023). The total procedural blank for chemical processing and measurement did not exceed ~60 ng K, which is negligible compared to the amount of K processed (~10–100 μg). Aliquots of geological reference materials, BHVO-2, W-2A, BCR-2, and JB-2 as well as aliquots of the NIST SRM3141a bracketing standard were also processed through all the chemical processing methods to monitor consistency with literature data and external reproducibility of measurements (Table 1).

3.2. Measurement of stable K isotopes

Potassium stable isotopic compositions of the samples were measured at the University of Bristol using 'Proteus', a unique tribrid collision cell multi-collector inductively coupled plasma mass spectrometer with pre-cell mass filter (CC-MC-ICPMS/MS) (Bevan et al., 2021; Lewis et al., 2022; Tacail et al., 2023).

Sample solutions were introduced to the plasma using a ~50 μl min^{-1} PFA nebuliser (ESI ST series) connected to an ESI APEX-Q desolvator. A standard sample cone and skimmer cone, with a 2.8 mm insert was used. The mass pre-filter is operated in full transmission mode and He and H_2 gases are introduced to the collision cell at 2 ml min^{-1} and 3.5 to 4 ml min^{-1} respectively (Tacail et al., 2023). Under these conditions Ar^+ based interferences, e.g., $^{40}ArH^+$ interference on ^{41}K, are charge neutralised while K^+ is transmitted and collisionally focussed through the collision cell, which allows for accurate measurement of $^{41}K/^{39}K$ in low mass resolution mode (M/ΔM ~3000, 5–95 % peak height definition) (Tacail et al., 2023). Argon intensity monitored at mass 38 (^{38}Ar) is similar to the monitored baseline intensity at mass 38.5 (~10^{-5} pA), reflecting its highly effective charge neutralisation.

The intensities of 6 masses were measured at the following mass-charge ratios: 38 (^{38}Ar), 38.5 (monitor baseline), 39 (^{39}K), 40 (^{40}Ca), 41 (^{41}K), and 42 (^{42}Ca) on Faraday cups L3 to H2 respectively. All cups were connected to amplifiers with 10^{11} Ω feedback resistors. Typical intensities for ~1 μg g^{-1} K solutions were ^{38}Ar < 0.001 pA, ^{39}K 250 to 300 pA, ^{40}Ca < 1 pA, ^{41}K 20 to 25 pA and ^{42}Ca < 0.01 pA. Typical $^{40}Ca/^{39}K$ ratios in samples were ~10^{-4} to 10^{-3} which corresponds to ^{40}Ca signals of between ~0.03 and 0.3 pA. High Ca content in K solutions may cause inaccuracies in data due to CaH^+ interreferences, namely $^{40}CaH^+$ on ^{41}K, which can be formed either in the ICP or the collision cell through interaction with H_2 collision gas. These interferences are not quantified here but under similar collision cell conditions on Proteus Lewis et al., (2022) found that the $^{40}CaH^+/^{40}Ca^+$

Table 1
Potassium isotopic composition of geological reference materials used in this study and literature data together with the reference solution standard processed through chemical separation. a – Pooled 2sd calculated for each measuring session. b – Two standard error calculated on pooled 2sd and n, for average sample compositions the 2se is calculated by adding the different samples 2se in quadrature. External reproducibility used for samples, calculated from repeat measurements of reference materials. c – n – Number of individual measurements. d – N – number of samples processed through chemistry and measured. e – Run as unknown. f – Literature data from the compilation in Wang et al. (2021). g – Average value in Parendo et al. (2022b). The literature compilation for BHVO-2 from Wang et al. (2021) (which we use to have a consistent data set for BCR-2 and W-2A) does not include data from Moynier et al. (2021) who report a BHVO-2 composition ($\delta^{41}K = -0.37 \pm 0.04$ ‰, 2sd, N = 5) similar to our measured composition.

Sample	Type	Measuring session	$\delta^{41}K$ (‰)	Pooled 2sd[a]	Pooled 2se[b]	n[c]	N[d]
NIST SRM3141a[e]	Bracketing standard	1	0.01	0.06	0.02	13	1
		2	−0.03	0.19	0.05	14	1
		Average	−0.01		0.03	27	2
BHVO-2	Basalt	1	−0.36	0.06	0.02	14	1
		2	−0.39	0.19	0.06	10	1
		Average	−0.38		0.03	24	2
BCR-2	Basalt	2	−0.45	0.19	0.04	20	1
JB-2	Basalt (arc lava)	1	−0.22	0.06	0.02	13	1
		2	−0.11	0.19	0.06	10	1
		Average	−0.16		0.03	23	2
W-2A	Dolerite	1	−0.47	0.06	0.01	34	1
		1	−0.44	0.06	0.01	25	1
		3	−0.43	0.12	0.03	13	1
		Average	−0.45		0.01	72	3
Literature				*2sd*		*N*	
BHVO-2[f]	Basalt		−0.46	0.09		108	
BCR-2[f]	Basalt		−0.49	0.18		86	
JB-2[g]	Basalt (arc lava)		−0.26	0.11		13	
W-2A[f]	Dolerite		−0.48	0.20		9	

production ratio is approximately 0.0001. Even given the highest measured ^{40}Ca beam intensities in sample K solutions this implies $^{40}CaH^{+}$ beam intensities of 0.03 fA which is a negligible contribution to the ^{41}K signal intensities.

The pre-cell, mass filter quadrupole, collision cell, and ion optics were tuned at the start of each session to achieve stability of K signal intensity and of $^{41}K/^{39}K$ ratios, aiming for an internal standard error of $\sim10^{-6}$ to 10^{-7} on $^{41}K/^{39}K$ measurements. Each analysis consists of 100 s of solution uptake to allow the ion beams to stabilise, followed by measurement of 40 cycles of 8.4 s integration time, consuming ~360 ng K per measurement. Sample and standard measurements were preceded and followed by 200 s of washing with 0.3 M HNO_3, followed by an 'on-peak' baseline measurement of reagent blank for 10 cycles of 8.4 s integration time. Typical reagent blank intensities were ^{39}K ~0.3 pA, ^{40}Ca ~0.005 pA, ^{41}K ~0.03 pA, ^{42}Ca < 0.0001 pA. Each sample was preceded and followed (after an 'on-peak' blank measurement) by a measurement of the NIST SRM3141a standard. The K standard was run at a K concentration of 1 μg g^{-1} and samples were matched in signal intensity to within 5 % of the standard. Each sample and standard were corrected for instrumental blank and intensities re-calculated. Samples were externally normalised to the bracketing solution standard and $\delta^{41}K$ calculated as $\delta^{41}K = [(^{41}K/^{39}K)_{sample}/(^{41}K/^{39}K)_{NIST\ SRM3141a} - 1]$ and reported in permille (‰).

3.3. External reproducibility and pooled variance

Samples and reference materials were measured in three, one week-long measurement sessions, one in November 2021 (session 1) that included Mariana arc lavas, and one in June 2022 (session 2) that included all sediment samples and some Mariana arc lava repeats (GUG6 and PAG3), and one in April 2024 (session 3) that included more Mariana arc lavas. For each measurement session we take a homoscedastic approach to determine precision (pooled 2sd) on any single K isotopic measurement, i.e., one standard-sample-standard measurement. This pooled 2sd is then used to calculate the standard error of the mean of repeat measurements of a given sample in that session. These data are reported in Tables 1, 2, and S2. We note however that our measurement sessions in November 2021 and April 2024 achieved better precision, than our session in June 2022; which relates to unstable measurement conditions following disassembly and reassembly (for cleaning purposes) of the collision cell on Proteus between measurement sessions 1 and 2 (see Lewis et al., 2022).

The calculated pooled 2se of the means individual sample measurements in sessions 1and 3 is ~0.03 ‰ while in session 2 it is a factor of two higher at ~0.06 ‰ reflecting the larger degree of variability in session 2 (Tables 1, 2, S2). The 2se provides a useful comparator of data quality between the runs but underestimates long term sample reproducibility.

Thus, we have also determined reproducibility by comparing averaged measurements of reference materials between measurement sessions, which is a more traditional assessment of reproducibility. Three separate samples (different dissolutions and column chemistry) of W-2A were measured (Table S2), in session 1 ($\delta^{41}K = -0.47 \pm 0.09$ ‰, 2sd, n = 34 and −0.44 ± 0.07 ‰, 2sd, n = 25) and in session 3 ($\delta^{41}K = -0.43$

Table 2
Potassium concentrations and isotopic compositions of samples measured in this study. a – Potassium concentration for Mariana arc lavas, average sediment unit compositions and bulk sediment is from Elliott et al. (1997) and individual Marine sediments are from Karpoff (1992), Plank and Langmuir (1998) and Vervoort et al. (2011). b – Pooled 2sd calculated for samples measured in different measuring sessions. c – Two standard error using pooled 2sd and n, for average sample compositions the 2se is calculated by adding the different samples 2se in quadrature. d – Sediment unit averages representative analytical uncertainty. e – Number of measurements and aggregated measurements. Bulk sediment composition calculated according to average unit compositions, sediment thickness and density following Plank and Langmuir (1998) and Elliott et al. (1997).

Group	Location	Sample	Lithology	[K] (ug g^{-1})[a]	$\delta^{41}K$ (‰)	Pooled 2sd[b]	Pooled 2se[c]	Sed. Unit 2sd[d]	n[e]
Mariana arc lavas central island province	Guguan	GUG3	Basalt	7538	−0.33	0.12	0.03		13
		GUG6			*−0.28*	*0.06*	*0.02*		*8*
		GUG6 replicate			*−0.29*	*0.19*	*0.06*		*10*
		GUG6 average	Basalt	3595	−0.29		0.03		18
		GUG9	Basalt	3590	−0.36	0.12	0.03		13
		GUG11	Basaltic andesite	4209	−0.23	0.06	0.02		8
		GUG12	Basaltic andesite	3719	−0.27	0.12	0.03		13
	Pagan	PAG1	Basalt	6281	−0.24	0.06	0.02		8
		PAG3			*−0.16*	*0.06*	*0.02*		*8*
		PAG3 replicate			*−0.19*	*0.19*	*0.06*		*10*
		PAG3 average	Basalt	6475	−0.17		0.03		18
	Agrigan	AGR2	Basalt	6176	−0.38	0.12	0.03		13
		AGR4b	Basalt	7090	−0.30	0.06	0.02		8
		AGR5	Basalt	7131	−0.41	0.12	0.03		13
		MM-92-6	Basaltic andesite	11,705	−0.31	0.06	0.02		8
	Ascuncion	ASC3ba	Basaltic andesite	4998	−0.35	0.12	0.03		13
	Uracas	URA5	Basaltic andesite	4400	−0.27	0.06	0.02		8
		URA7	Basaltic andesite	6276	−0.28	0.06	0.02		8
		URA12	Basaltic andesite	5853	−0.33	0.12	0.03		13
Marine sediment	ODP site 801	801A-3R2-56-58	Pelagic clay	34,452	−0.37	0.19	0.06		10
		801A-5R3-50-51	Pelagic clay	35,448	−0.37	0.19	0.06		10
		Unit 1	Brown clay	32,625	−0.37			0.09	
		801A-80-100M	Chert	6309	−0.43	0.19	0.06		10
		Unit 2	Chert + Pc	6392	−0.43			0.09	
		801A-17R1-28-30	Porcellanite	12,203	−0.83	0.19	0.06		10
		801B-5Rl-40-42	Volcaniclastic	13,283	−1.32	0.19	0.06		10
		801B-7R1-34	Volcaniclastic	31,297	−1.43	0.19	0.06		10
		Unit 3	Volcaniclastic	13,449	−1.28			0.09	
		801B-15R1-19-20	Chert	8883	−0.60	0.19	0.06		10
		801B-24R1-54-112	Radiolarite	7804	−0.47	0.19	0.06		10
		801B-35R2-0-10	Rad + Clst	22,580	−0.43	0.19	0.06		10
		Unit 4/5	Rad + Clst	5022	−0.48			0.09	
		Bulk sediment		10,053	−0.85			0.09	

± 0.08 ‰, 2sd, n = 13), with an external reproducibility of δ^{41}K ± 0.05 ‰, 2sd, N = 3, where N is the number of full replicate measurements. We use this external reproducibility for data measured in sessions 1 and 3. Given the factor of two less precise data measured in session 2 relative to sessions 1 and 3 (0.06 ‰ vs 0.03 ‰, pooled 2se) we similarly scale our estimate of external reproducibility appropriately by a factor of two (i.e., δ^{41}K ± 0.09 ‰, 2sd) for samples analysed in session 2. Repeat measurements of BHVO-2, JB-2, GUG6, and PAG3 measured in sessions 1 and 2 are consistent with uncertainty (Tables 1 and 2), i.e., the reproducibility for each of the two sessions combined in quadrature (±0.05 ‰, 2sd). Measurements of NIST SRM3141a processed through chemical purification methods average at −0.01 ± 0.05 ‰, 2sd, (n = 27 individual measurements of two different aliquots processed separately through chemistry and analysed in two different sessions), indicating the lack of column fractionation effects. All data on reference materials are within uncertainty of literature data (Table 1). For sediment unit average compositions and the bulk sediment composition we ascribe a representative analytical uncertainty of δ^{41}K ± 0.09 ‰, 2sd, (Table 2), as all sediment samples were measured in session 2.

4. Results

4.1. Mariana arc lavas

The K concentrations of Mariana arc lavas measured in this work range from ~3600 to 12,000 ug g^{-1} (Table 2), and are enriched up to around an order of magnitude relative to mean fresh normal (N)-MORB (1300 ug g^{-1} Gale et al., 2013). The stable K isotopic compositions of the Mariana arc lavas range from δ^{41}K = −0.41 to −0.17 ‰, extending from near MORB compositions (δ^{41}K = −0.44 ± 0.09 ‰, 1sd, Tuller-Ross et al., 2019b) to isotopically heavier than the ODP site 801C AMOC supercomposite (δ^{41}K = −0.32 ± 0.04 ‰, 2sd, Hu et al., 2020). There are no systematic variations between K concentration and δ^{41}K with tracers of magmatic differentiation such as SiO_2 and MgO (Fig. S2). There is a positive correlation in the ratios of fluid mobile to fluid immobile elements of similar incompatibility, such as K/La and Ba/Th (Fig. 5a), indicating the fluid addition of Ba and K to the Mariana arc lava source. There is also a positive trend, shown in a regression line (Fig. 5b), between K/La and δ^{41}K where the isotopically heaviest samples, GUG11 and PAG3, have highest fluid mobile/fluid immobile ratios (Fig. 5b). This indicates that fluids may be a source of isotopically heavy K in the Mariana arc lavas.

4.2. Mariana arc sediments

Sediment samples extend to isotopically lighter compositions than the Mariana arc lavas, and AMOC from the same site (Fig. 5b). There is a large range in δ^{41}K of the sediments (~1 ‰) ranging from δ^{41}K = −1.4 ‰ in a volcaniclastic sediment to −0.37 ‰ in a pelagic clay (Fig. 5b). Potassium concentrations show a large range, ~6300 to 35,000 ug g^{-1}, with highest values in the pelagic clays (Table 2). Average sediment units and bulk sediment have lower K/La ratios than the Mariana arc lavas and a large range in Ba/Th (Fig. 5a). The volcaniclastic samples also have the highest K/La ratios, bar one sample from the radiolarite and claystones, and they are also the isotopically lightest (Fig. 5b), which may indicate K addition with isotopic fractionation, where isotopically light K is preferentially incorporated into sediments (Hu et al., 2020).

The discrete sediment samples can be grouped into their respective units and a K isotopic composition calculated from an average, weighted by their K concentrations (Table 2). Trends of the discrete samples and the average compositions for the units are generally the same. Therefore, unless otherwise stated, any further discussion of ODP site 801 sediment samples will relate to the average compositions of the units. Samples from the Pelagic clay, Chert and Porcellanite, and Radiolarites & Claystone units are indistinguishable from MORB in δ^{41}K (Fig. 5b). The Volcaniclastic unit however is significantly isotopically lighter than any other of the Mariana arc inputs (Fig. 5b). The bulk sediment composition (dominated volumetrically by the volcaniclastic component) has a K concentration slightly lower than the volcaniclastic component, but more enriched than chert and porcellanite and radiolarites & claystone, low Ba/Th and K/La and is isotopically light and distinguishable from the Mariana arc lavas, MORB and AMOC (Fig. 5). The estimate of the subducting sedimentary column in this study is more representative of the bulk sedimentary composition subducted at the Mariana arc than previous data from the study from Hu et al. (2020). Their estimate is

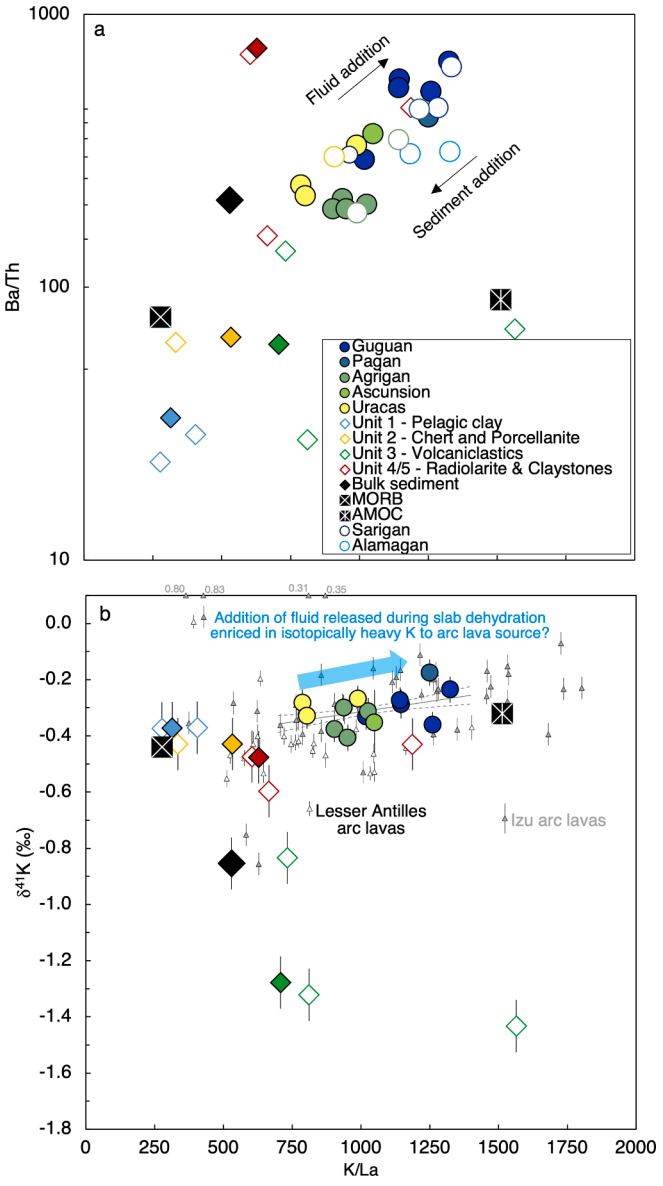

Fig. 5. (a) Ba/Th vs. K/La ratios for the full set of Mariana arc lavas from Elliott et al. (1997). Symbols are the same as in Fig. 4. Hollow circles with coloured outlines are arc lavas without δ^{41}K measurements. Arrows indicate the inferred effects of fluid and sediment addition to Mariana arc lava sources. (b) δ^{41}K vs. K/La, error bars are the external reproducibility. Symbols are the same as in Fig. 4. A weighted linear regression with an error envelope through the Mariana arc lavas is shown as thin grey lines and shows a positive correlation with δ^{41}K and K/La. The blue arrow schematically shows the enrichment of isotopically heavy K in Mariana arc lavas inferred for a fluid released by subducting slab dehydration. Izu and Lesser Antilles arc lavas are included as small grey and white triangles from Parendo et al. (2022b) and Hu et al. (2021a) respectively.

based on the composition of the 'SED' component from Kelley et al. (2003) which is a composite of interflow sediments accumulated between basaltic pillows in the upper 230 m of igneous basement and has a K isotopic composition of −0.42 ± 0.06 ‰, 2sd, identical to fresh MORB (Tuller-Ross et al., 2019b; Hu et al., 2020). This 'SED' sample is not representative of the entire sedimentary column.

5. Discussion

5.1. Controls on the K isotopic composition of arc lavas and sediments

The high concentrations of K in subduction zone inputs (ODP 801 sediments [K] ~10,000 ug g^{-1} and AMOC [K] ~5300 ug g^{-1}) relative to the low concentration of the depleted MORB source ([K] ~60 ug g^{-1}) (Salters and Stracke, 2004), means that the addition of a small amount of slab-derived components (i.e., aqueous fluid released from the dehydration of the subducting slab and subducting sediments) should strongly alter the composition of the sub-arc mantle. However, first it is necessary to assess other factors such as magmatic differentiation that may alter K isotopic compositions.

The Mariana arc lavas represent a suite of basaltic-to-basaltic andesite lavas that have undergone magmatic differentiation to MgO contents varying from 6.2 to 2.3 wt%. The lavas are porphyritic, with xenocrysts of olivine and phenocrysts of plagioclase, clino/*ortho*-pyroxene and titanomagnetite and are not true liquid compositions (Elliott et al., 1997). Resolvable K isotopic fractionations, ~1 ‰, have been reported in evolved felsic systems due to the continuous separation and crystallisation of phases such as plagioclase, hornblende, biotite, K-feldspar, and muscovite that may take up heavy K isotopes (Zeng et al., 2019; Kuhnel et al., 2021; Wang et al., 2022; Ding et al., 2023; Huang et al., 2023), however, no resolvable fractionation has been reported in basaltic lavas. Results from Tuller-Ross et al. (2019a) and Hu et al. (2021b) on basaltic lavas from Hekla Iceland and Kilauea Iki lava lake Hawaii respectively show no resolvable K isotopic fractionation during magmatic differentiation ranging from MgO contents 26.9 to <1 wt%, due to low K concentrations in major crystalising phases in mafic magmas (olivine and pyroxene) (Wang et al., 2022).

Moreover, the lack of systematic variations in δ^{41}K or K/La of the Mariana arc lavas with SiO_2 and MgO (Fig. S2) implies that any variability in the δ^{41}K composition of Mariana arc lavas likely represents source heterogeneity in the sub-arc mantle wedge. Given that most of our Mariana arc lavas have δ^{41}K resolved from MORB (Fig. 5b), they likely reflect the contribution of isotopically distinct components that have been added to the sub-arc mantle wedge. The addition to the sub-arc mantle wedge of a near constant flux of an aqueous fluid released from the dehydration of the subducting slab has long been invoked to explain the elemental and isotopic composition of Mariana arc lavas (e.g., Elliott et al., 1997). Given other data (e.g., from the Sumdo eclogites Liu et al., 2020; Lesser Antilles arc Hu et al., 2021a; Izu arc Parendo et al., 2022b; and Avacha mantle wedge peridotites Wang and Ionov, 2023) suggests that isotopic fractionation of K occurs during slab dehydration, we first asses this as a cause for the K concentration and isotopic compositions of our Mariana arc lava samples.

5.2. Aqueous fluid component

As discussed earlier, we envisage an aqueous, oxidised fluid component derived from the dehydration of serpentinites at the base of the subducting slab, that flows through reactive channelised flow and samples the mafic oceanic crust leaching fluid mobile elements (Ulmer and Trommsdorff, 1995; Peacock, 2001; Zack and John, 2007; Spandler et al., 2011; van Keken et al., 2011; John et al., 2012; Freymuth et al., 2015, 2016; Chen et al., 2019b; Freymuth et al., 2019; Klaver et al., 2020; Stubbs et al., 2022). In subducting mafic oceanic crust K will dominantly be hosted within phengite (K_2O up to 11 wt%) and amphibole (K_2O up to 0.2 wt%) (Liu et al., 2020). In partitioning between a fluid and solid phase the light ^{39}K isotope is preferentially retained in the solid, while isotopically heavy ^{41}K is released to the fluid, as seen in continental weathering processes and inferred from high temperature eclogites (Li et al., 2019a, 2019b; Zeng et al., 2019; Chen et al., 2020; Hu et al., 2020; Huang et al., 2020; Teng et al., 2020; Liu et al., 2020). Heavy isotopes are preferred in phases with stiffer bonds, typically with lower coordination numbers (Schauble, 2004). In aqueous solutions K has the potential to be in a lower coordination number, 6 ± 2, than in potential hosts for K in subducting oceanic crust, e.g., phengite, omphacite, and amphibole in which K sits in 6, 7 to 8 and 8 co-ordinated sites respectively (Huebner and Papike, 1970; Hawthorne and Calvo, 1977; Li et al., 2019b). Therefore, there is potential for K isotopic fractionation during dehydration of a subducting slab with relative enrichment of ^{41}K in the fluid phase (Liu et al., 2020; Hu et al., 2021a; Parendo et al., 2022b; Wang and Ionov, 2023).

Following Liu et al. (2020), who model the composition of the exhumed Sumdo eclogites via a Rayleigh fractionation model to dehydrate the subducting slab and following the formulation outlined in Chen et al. (2019b) and Stubbs et al. (2022) where the fluid is modelled as an accumulating fluid subject to Rayleigh isotopic fractionation (full list of model details is provided in the Supplementary Material), we model the K isotopic composition of an aqueous fluid sourced from the dehydration of the subducting slab that passes up through the crust and leaches fluid mobile elements, with residual amphibole, omphacite and phengite as the crustal hosts for K. We use an average modal abundance of amphibole, omphacite and phengite from the Sumdo eclogites in Liu et al. (2020). We also use solid–fluid partition coefficients, $D^{K}_{Solid/Fluid}$, from Zack et al. (2001) and Liu et al. (2019, 2020). We note that there is no source of partition coefficients derived for omphacite and use the value quoted in Liu et al. (2020); given its low value (0.002) and low relative K concentration ~0.01 wt%, omphacite has little effect on the K budget.

For an initial down going igneous oceanic crust K concentration and δ^{41}K composition we use a weighted mean between AMOC and unaltered oceanic crust. We assume 6000 m of oceanic crust and treat the upper 500 m as AMOC, using the ODP 801C supercomposite K concentration and δ^{41}K composition from Hu et al. (2020). An unaltered oceanic crust composition, from White and Klein (2014), is used for the rest of the subducting crust. It is assumed that the K in the aqueous fluid phase is sourced from the whole oceanic crust (Avanzinelli et al., 2012). Full list of model parameters is given in Tables S3–S7.

The K concentration of the released fluid is modelled against the concentration of the fluid immobile element La. We use La partitioning data from the RK200 800 °C 4 GPa experiment from Kessel et al. (2005). Water content for the subducting slab of 1 wt. % to 6 wt. % is assumed (Schmidt and Poli, 1998), and all of this is lost to the mantle wedge to account for unknown amounts of dehydration. Perhaps the most significant uncertainty in the model is the K isotopic fractionation factor between the solid residue and the released fluid $\alpha(^{41}K/^{39}K)_{solid/fluid}$. There is a lack of experimental data for K isotopic fractionation factors. Liu et al. (2020) use a $\alpha_{solid\text{-}fluid}$ value of 0.9985, based on a best fit to data. They argue that such large inferred fractionations are in keeping with the work of Morgan et al. (2018) who reported fractionations > 1 ‰ in δ^{41}K in 'high-temperature', igneous rocks associated with high fluid contents (such as pegmatites between minerals such as K-feldspar, micas, and astrophyllite). Parendo et al. (2022b) however use a $\alpha_{solid\text{-}fluid}$ value of 0.9996 to 0.9995 based on a best fit to data to generate K isotopic compositions in the Izu arc, which is a more comparable geological setting to our Mariana arc lava samples. We primarily adopt a fractionation factor of 0.9996, but also test models with other fractionation factors.

The Mariana sub-arc mantle (MSM) is modelled from a depleted MORB mantle composition from Salters and Stracke (2004) using an accumulating, fractional non-modal melting model, using partition coefficients from Salters and Stracke (2004) and modal abundances and melt modes from Robinson et al. (1998) (Table S6). The Mariana arc lava

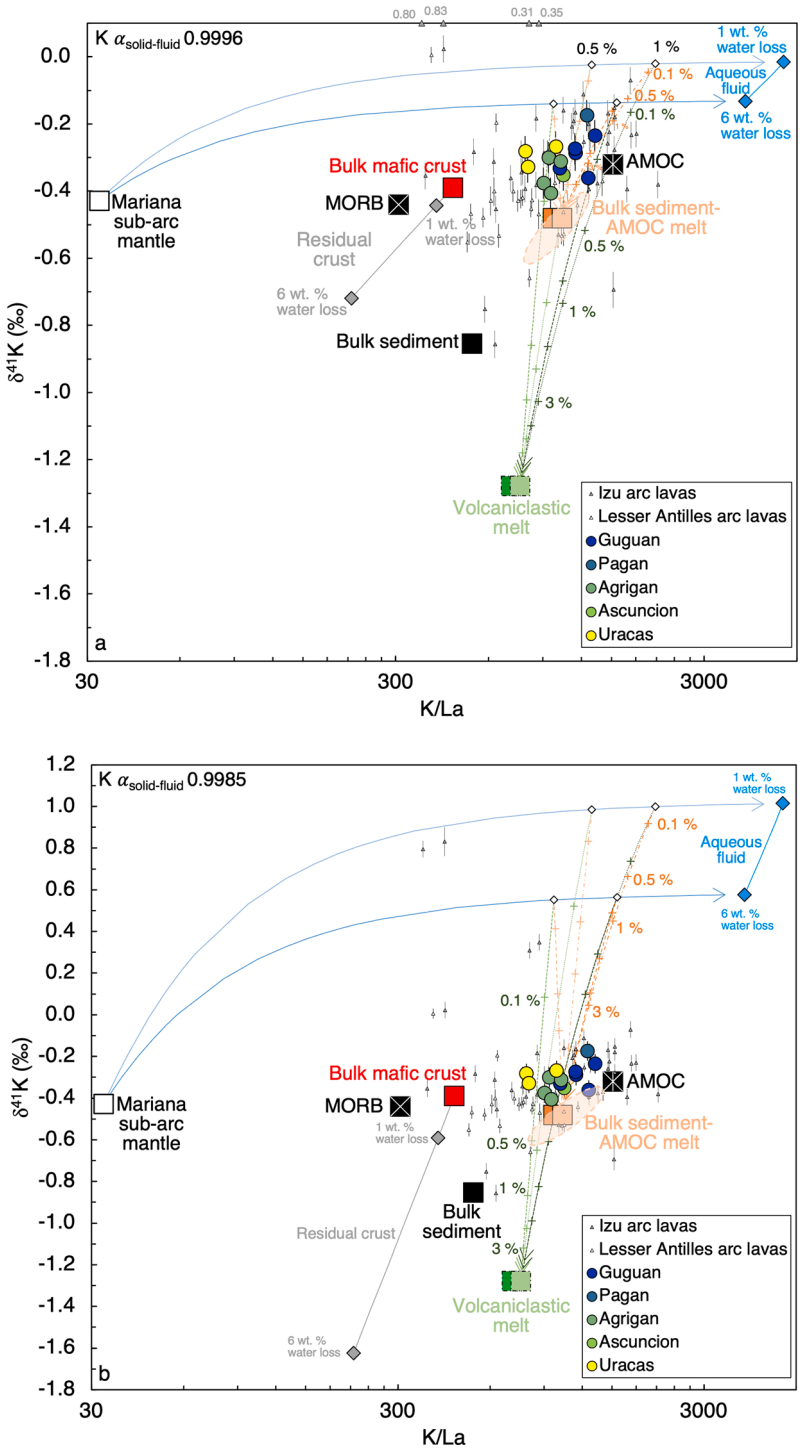

Fig. 6. Models of aqueous fluids from slab dehydration and a sediment component melt that is either volcaniclastic material or bulk sediment with AMOC, mixed into the MSM in δ^{41}K vs. K/La space. The K isotopic composition of fluids released during dehydration is controlled by $\alpha_{solid\text{-}fluid} = 0.9996$ in (a), $\alpha_{solid\text{-}fluid} = 0.9985$ in (b) and $\alpha_{solid\text{-}fluid} = 0.9998$ in (c). Bulk mafic crust starting composition is a concentration and thickness weighted average of the mafic oceanic crust and AMOC. (a–c) Light and dark blue shaded lines represent released aqueous fluid from the dehydration of the subducting slab that loses 1 wt. % and 6 wt. % water respectively, of an initial 6 wt. % water content (blue diamonds) and is mixed into the MSM in indicated (white diamonds) proportions. Grey diamonds and line represent the composition of the residual crust following dehydration. Orange (bulk sediment with AMOC) and green squares (volcaniclastic) represent the compositions of the sediment component (darker colours) and sediment component melt (pastel colours). Mixing trajectories of a sediment component melt mixed into the MSM metasomatized by fluid addition are shown as either shades of orange (bulk sediment with AMOC) or green (volcaniclastic). Lighter and darker orange and green shades when sediment component melt is added to MSM metasomatized with a 0.5 % and 1 % fraction of the modelled aqueous fluid respectively. Dash-dot and dash lines are for mixing of the sediment component melt with MSM metsomatised with the modelled aqueous fluid derived from 1 to 6 wt. % water loss of the subducting slab respectively. Orange shaded ovals represent potential endmember compositions of the melted bulk sediment-AMOC mixture, given uncertainty in Pb-Pb systematics in Fig. 2. Mixing proportions of the sediment component melt are shown as orange or green crosses in 0.1, 0.5, 1, and 3 % fractions. Izu arc lava samples are shown as small grey triangles and are from Parendo et al. (2022b), and Lesser Antilles arc lava samples as small white triangles and are from Hu et al. (2021a). Error bars on Mariana arc lavas are the external reproducibility 2sd.

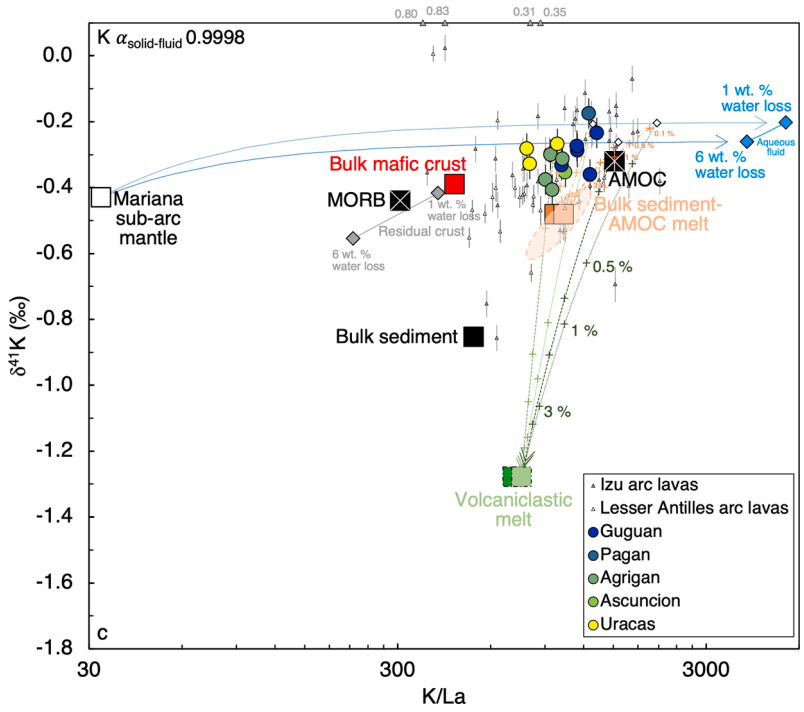

Fig. 6. (*continued*).

mantle source is melted ~2 % following Elliott (2003) and then the released fluid is mixed into it and the final composition calculated from mass balance. The H_2O contents of primary olivine hosted fluid inclusions in lavas from Guguan are well constrained, ~3 to 4.5 wt. % (Kelley et al., 2010). If the mantle source melts ~20 % (Kelley et al., 2010) and assuming all H_2O goes into the accumulating melt, then the amounts of fluid mixed into the MSM source should be ~0.5 to 1 % (Stubbs et al., 2022). Therefore, we mix 0.5 and 1 % of the released fluid into the arc lavas source and melt the final mixture by 20 % using an accumulating fractional non-modal melting equation to model Mariana arc lava compositions.

Our modelled fluids extend from $\delta^{41}K = -0.02$ ‰ to −0.13 ‰, for scenarios of between 1 wt. % and 6 wt. % water loss from the subducting slab (i.e., total water loss given an initial 6 wt. % water, which corresponds to a fraction loss of ~0.166 to 1) (Fig. 6a). Estimates of the amount of water that makes it past the subduction zone filter and further into the mantle, or conversely, the amount lost during dehydration, is highly debated (e.g., Jarrard, 2003; Hacker, 2008; van Keken et al., 2011) and varies up to near total dehydration (e.g., Dixon et al., 2002), therefore we find it reasonable to use a large range in our models to show endmember cases. The fraction of K lost from the oceanic crust during dehydration is 13 to 56 % for 1 wt. % to 6 wt. % water loss models respectively (Fig. 6a). Due to the low concentrations of K in the MSM and high concentration of K in the released fluid, e.g., ~13,000 to 10,000 ug g^{-1} for 1 wt. % to 6 wt. % water loss, small amounts of fluid addition significantly perturb the K/La ratio and K isotopic composition of the sub-arc mantle. Ratios of K/La in the Mariana arc lavas range from ~800 to 1300 and can be re-created with a fraction of between 0.5 % to 1 % (i.e., water contents of arc lavas of 2.5 to 5 wt. % given 20 % melting) of the released fluid in the arc lava source, with lavas from Uracas requiring smaller amounts of fluid added to their mantle source (Fig. 6a). Mixing curves tracking fluid addition alone to MSM are too isotopically heavy to match the Mariana arc lavas (Fig. 6a); as expected from other elemental systematics, another component added to the sub-arc mantle wedge is needed, i.e., an isotopically low $\delta^{41}K$ composition with high K/La, such as subducting sediments.

Before considering the sediment component, we note that our

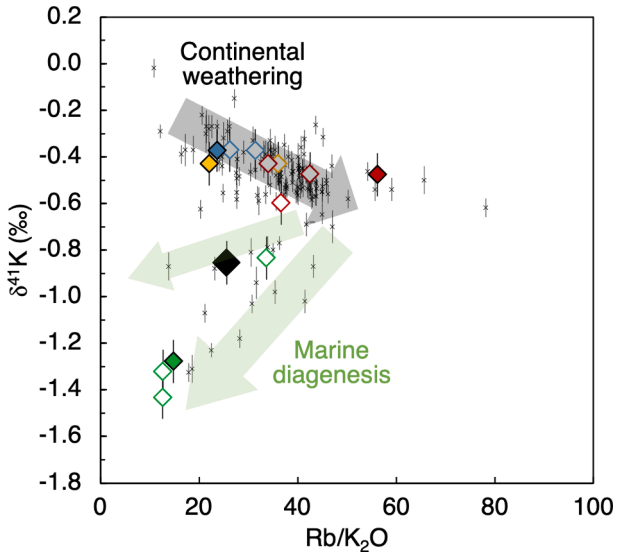

Fig. 7. $\delta^{41}K$ vs. Rb/K_2O showing ODP site 801 sediment samples plotted in the same symbols as Fig. 4 and data compiled from literature for weathered continental rocks and other Marine sediments (Carpentier et al., 2008; Vervoort et al., 2011; Chen et al., 2020; Huang et al., 2020; Hu et al., 2020, 2021a; Teng et al., 2020; Parendo et al., 2022a). Grey arrow represents the direction continental weathering drives compositions and green arrows the direction marine diagenesis drives compositions. Re-created and modified from Hu et al. (2020).

modelling results depend on the choice of fractionation factor between solid and fluid for the isotopic composition of the released aqueous fluid. For example, if a larger fractionation factor, $\alpha_{solid\text{-}fluid}$ 0.9985, is used then modelled fluids extend to much higher $\delta^{41}K$ up to 1 ‰, too isotopically heavy to match the Mariana arc lavas (Fig. 6b). If a smaller fractionation factor, $\alpha_{solid\text{-}fluid}$ 0.9998, is used (an estimate to best fit data with an aqueous fluid component alone), then between 0.5 to 1 % of aqueous fluid added into the MSM can re-produce more of the Mariana arc lavas, for example some samples from Guguan, Pagan, and Uracas

(Fig. 6c), without the need of a sediment component. However, using this alternative fluid composition some of the lavas from Agrigan and isotopically lightest samples are still not reproduced (Fig. 6c). Therefore, a model that accounts for all arc lava samples likely requires a sediment component, consistent with previous geochemical inferences. It is also worthwhile to mention that we opt to not model a mélange mix and melt model that has been proposed to reconcile some features of arc lava geochemistry (e.g., Nielsen and Marschall, 2017). Maunder et al. (2024) show that Br/Cl and I/Cl ratios of the Mariana arc lavas better fit with a model of subducting slab dehydration rather than a mélange mix and

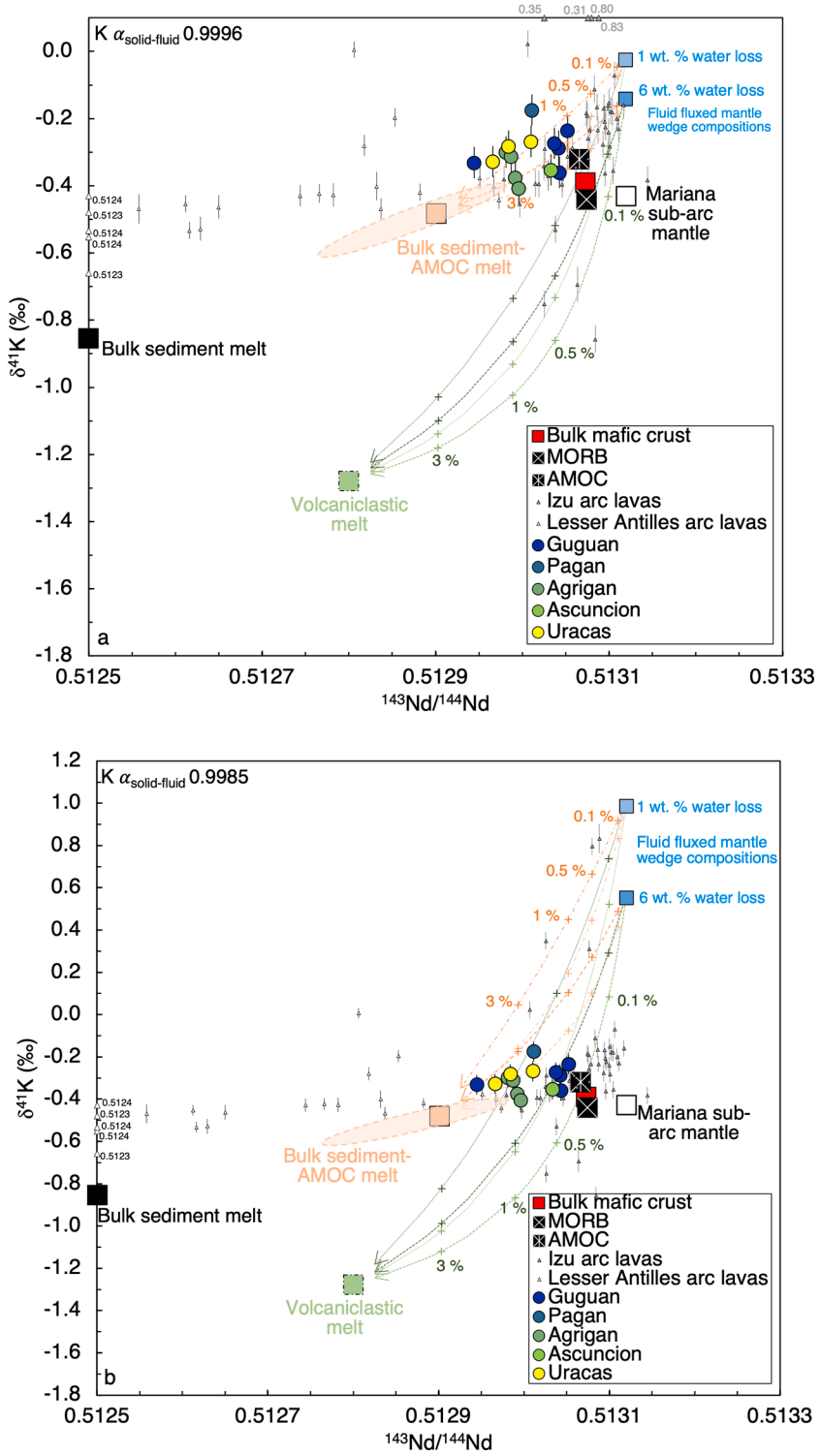

Fig. 8. Mixing model of slab dehydration and sediment melt component mixed into the MSM to create the Mariana arc lavas in δ^{41}K vs. ^{143}Nd/^{144}Nd space. Details of model and parameters used are given in the main text and Supplementary Material and Tables S3–S7. Model uses different fractionation factors for K during slab dehydration (a) $\alpha_{solid\text{-}fluid} = 0.9996$ (b) K $\alpha_{solid\text{-}fluid} = 0.9985$, (c) $\alpha_{solid\text{-}fluid} = 0.9998$. Figure details are the same as described in Fig. 6. Fluid modified mantle wedge compositions are shown as light blue and dark blue squares for MSM compositions mixed with 0.5 % and 1 % (data points overlap at this scale) of an aqueous fluid from a subducting slab that has lost 1 wt. % and 6 wt. % water respectively.

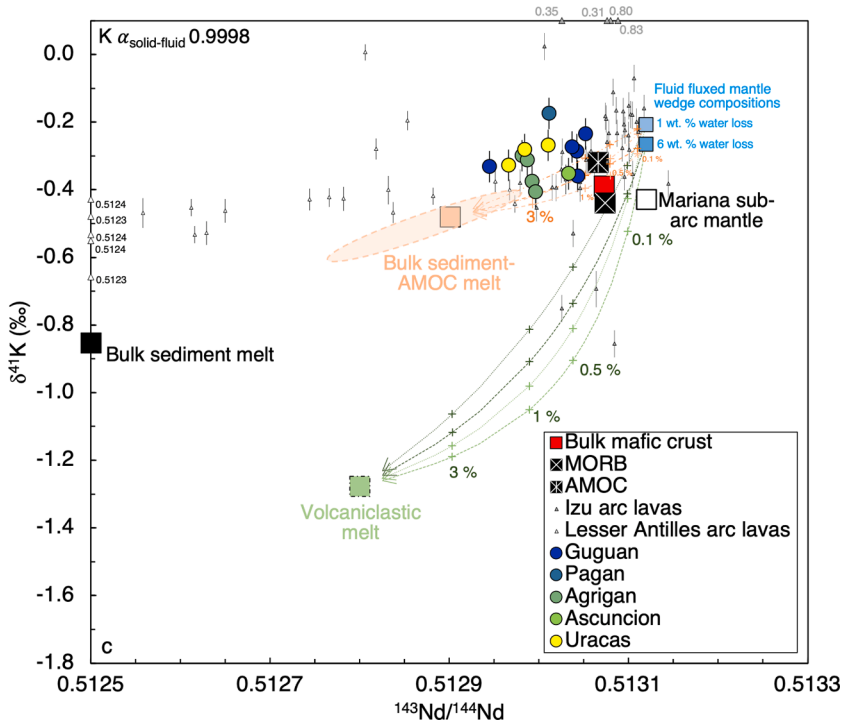

Fig. 8. (*continued*).

melt model, and therefore we chose to focus on traditional fluid/melt-mantle metasomatism models in this section.

5.3. Nature of the sediment component

As discussed in Section 1, the sediment component added to the source of Mariana arc lavas is likely either a volcaniclastic component or a mix of bulk sediment and AMOC mixed in correct proportions to fit with inferences from Pb-Pb systematics (Fig. 2) (Tollstrup and Gill, 2005; Avanzinelli et al., 2012; Freymuth et al., 2015). Note that we use the term sediment component for simplicity to count as either the volcaniclastic component or mix of bulk sediment and AMOC. For this mixture of bulk sediment and AMOC, the incompatible trace element budget of some elements, such as Pb, is dominated by the bulk sediment fraction. For K, on average ~30 % is sourced from bulk sediment and 70 % from AMOC but given uncertainty in the composition of the bulk sediment, may vary from ~16 to 56 % K sourced from bulk sediment (Fig. 2). Given the distinct K isotope ratios of the volcaniclastic unit and bulk sediment-AMOC there is the potential to distinguish between these different components added to the source of the Mariana arc lavas. The volcaniclastic sediment is the only individual sediment unit distinguishable from MORB and because it biases the bulk sediment composition it is worth exploring why it is distinctly isotopically light in K.

From a global study, Hu et al. (2020) show that marine sediments, that are a mix of detrital, biogenic, and authigenic phases, largely fall on a negative array in a plot of δ^{41}K vs Rb/K_2O (Fig. 7). The trend to low δ^{41}K and higher Rb/K_2O is indicative of continental weathering, where lighter K isotopes and a larger cation, Rb relative to K, are favoured in clay mineral formation. Units 1, 2, and 4/5 fall on this well-defined trend line (Fig. 7) reflecting the dominance of continental weathering; however, the volcaniclastic unit falls off this trend line and extends to low Rb/K_2O and extremely low δ^{41}K. This, as seen in some other marine sediments (Hu et al., 2020) and notably in other volcaniclastic samples outboard of the Izu-Bonin trench (e.g., C0011D-16H-6-W-113–115 volcanic ash δ^{41}K: −1.3, Rb/K_2O: 18 Parendo et al., 2022a), is interpreted by Hu et al. (2020 and references therein) to reflect the diagenetic

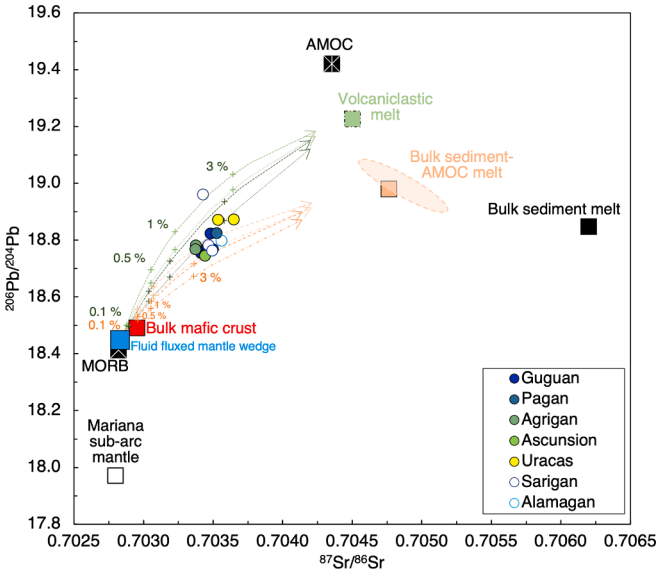

Fig. 9. Mixing model of slab dehydration and sediment melt component mixed into the MSM to create the Mariana arc lavas in ^{206}Pb/^{204}Pb vs. ^{87}Sr/^{86}Sr space. Details of model and parameters used are given in the main text and Supplementary Material and Tables S3–S7. Figure details are the same as described in Fig. 6. Fluid fluxed mantle wedge compositions are shown as a blue square for MSM compositions mixed with 0.5 % and 1 % of an aqueous fluid from a subducting slab that has lost 1 wt. % and 6 wt. % water (data points overlap at this scale).

uptake of isotopically light K during the formation of authigenic minerals such as glauconite during *in-situ* marine weathering of originally anhydrous volcaniclastics. Authigenic marine minerals such as illite and glauconite become enriched in isotopically light K relative to seawater, potentially due to lower K-O bond strength in clays relative to hydration in solution, faster diffusion of ^{39}K to the surfaces of growing clays, and

preferential loss of ^{41}K during hydrated K desolvation (Bourg et al., 2010; Hofmann et al., 2012; Santiago Ramos et al., 2018; Zeng et al., 2019; Huang et al., 2020; Hu et al., 2020; Li et al., 2022).

We choose to model the sediment component as a melt, as there has been a large amount of evidence to support the melting of subducting sediments and potentially AMOC in subduction zones, e.g., enrichments in fluid immobile Th that is sourced from sediments relative to Nb due to the retention of Nb in rutile in sediments that melt (e.g., Brenan et al., 1994; Plank and Langmuir, 1998; Johnson and Plank, 2000; Elliott, 2003; Kessel et al., 2005; Plank, 2005, 2014; Skora and Blundy, 2010; Klaver et al., 2020; Turner and Langmuir, 2022).

We therefore model the sediment component as a melt of either a pure volcaniclastic sediment or a mix of bulk sediment and AMOC, that we then mix with the fluid fluxed MSM, that then further melts by ~20 %. We use the bulk partition coefficients from Martindale et al. (2013), who specifically performed melting experiments on a volcaniclastic sediment from ODP 801. We use their experiment vc4, melted at 3 GPa and 850 °C. Lanthanum under these conditions has a $D_{sediment\text{-}melt}$ of 0.72 and is similar to K, $D_{sediment\text{-}melt}$ 0.60, which both become enriched in the melt (Martindale et al., 2013). We use a melt fraction of 67 % for the melt component, given data in experiment vc4 from Martindale et al. (2013), which is in line with other works that suggest high degrees of sediment melting (Schmidt et al., 2004; Spandler et al., 2007; Skora and Blundy, 2010; Turner and Langmuir, 2022). However given the similar incompatibility of K and La under these conditions during sediment melting, both are enriched with a fraction of ~80 % in the melt and the K/La ratio increases slightly between the sediment component and sediment component melt. Therefore, the degree of melting has little control over the modelled compositions. Given the significant loss of K from sediment to melt due to its incompatible nature and distinctly light isotopic compositions we assume isotopic fractionation of K during melting likely insignificant and assume that the $\delta^{41}K$ of the sediment melt will resemble its source. We also assume the same $D_{sediment\text{-}melt}$ for bulk sediment-AMOC mix melting, as again K and La with similar behaviour are likely to be enriched by similar degrees and therefore the K/La ratio will change by a small amount. This melting increases the K/La ratio from ~700 and 950 to ~750 and ~1000 for melts of volcaniclastic and bulk sediment-AMOC mix respectively (Fig. 6).

Mixing either sediment melt component, that is isotopically lighter than the Mariana arc lavas, with fractions up to ~3 % and just over, to a fluid modified MSM can reproduce many of the Mariana arc lava compositions (Fig. 6a). Model results are shown with a sediment melt component endmember added to a fluid released from a slab that has lost 1 wt. % and 6 wt. % water, and then mixed with the MSM in 0.5 and 1 % proportions (Fig. 6a). These mixing trajectories bracket many of the Mariana arc lavas and thus can represent upper and lower bounds of sediment and fluid addition to the MSM needed to generate the arc lavas; therefore, even if a sample does not fall on the specific mixing trajectories shown, it should fall on a line between these bounds. Given the uncertainty in the mixing proportions of the bulk sediment and AMOC mix (Fig. 2) there is a small range in potential end-member compositions for our illustrated mixing models. We chose to show this has an orange oval in Figs. 6, 8, and 9, that ranges from ~9 to 37 % mass fraction of bulk sediment, average of 18 % (with 16 to 56 % of the K budget of the bulk sediment – AMOC mixture from the bulk sediment) (Fig. 2), and note that the end points of modelled mixing curves may fall within this range (Figs. 6, 8, and 9).

Some of the lavas from Guguan and Pagan have less of a sediment melt component than Uracas, Agrigan and Ascunsion for example, and more strongly show the influence of the slab derived fluid component (Fig. 6a). The lowest K/La lavas from Uracas are not reproduced with a volcaniclastic melt component endmember. However, with a bulk sediment-AMOC mix melt endmember these samples could potentially be reproduced, with higher amounts of bulk sediment in the bulk sediment AMOC mixture, a possibility given uncertainty in the Pb-Pb compositions from which the mixing proportion is calculated (Figs. 2 and 6a). In the model case, with $\alpha_{solid\text{-}fluid}$ 0.9985, the lowest and highest K/La samples are not reproduced with a volcaniclastic melt component endmember (Fig. 6b). The bulk sediment-AMOC mix melt endmember can reproduce more of the arc lavas with the variability in mixing proportions but is still not able to reproduce many of the arc lavas at a fixed shown mixture between bulk sediment and AMOC, with the endmember composition either having too low or high K/La to intercept most of the arc lavas (Fig. 6b).

In the model with a smaller isotopic fractionation, $\alpha_{solid\text{-}fluid}$ 0.9998, the volcaniclastic melt component again does not reproduce the lowest K/La samples, nor with the bulk sediment-AMOC mix even given the potential variability in the mixing proportions (Fig. 6c). Therefore in $\delta^{41}K$ – K/La space it is possible to recreate the Mariana arc lavas generally better with a $\alpha_{solid\text{-}fluid}$ of 0.9996 and sediment component melt of bulk sediment with AMOC, in contrast to previous studies that suggest a volcaniclastic component (e.g., Avanzinelli et al., 2012). Models also re-create variations between the islands (Fig. 5b) where some lavas from Guguan and Pagan have slightly higher K/La and higher $\delta^{41}K$ than some from Uracas and Agrigan, due to variable sediment contributions. However given some of the uncertainty in the model and variations in mixing proportions between bulk sediment and AMOC, we further test our models by modelling the K isotopic composition with the radiogenic $^{143}Nd/^{144}Nd$ composition, which like $\delta^{41}K$ shows significant difference between the bulk sediment and volcaniclastic components (Fig. 8) (Elliott et al., 1997).

Mariana arc lavas are all relatively radiogenic in $^{143}Nd/^{144}Nd$, with compositions > 0.5129, with the sediment-poor islands being slightly more radiogenic than the sediment rich islands (Fig. 8). We use the same modelling approach as above using parameters in Tables S3–S7. The MSM Nd isotopic composition is from Woodhead et al. (2012). For the Nd isotopic composition of the released fluid we use the Nd isotopic composition of the concentration weighted oceanic crust, where the isotopic composition is from Gale et al. (2013) and AMOC from Hauff et al. (2003) (Average 801 igneous crust, volume and concentration weighted). Experimental data for element partitioning data between eclogite and fluid from Kessel et al. (2005) is used for the elemental partitioning of Nd.

Our model results (Fig. 8) show that the Nd and K isotopic compositions of many of the Mariana arc lavas can be better reproduced, with similar proportions to those in the $\delta^{41}K$ – K/La model (Fig. 6) (up to ~3 % and just over), with the addition a melted bulk sediment-AMOC component with a fractionation factor of $\alpha_{solid\text{-}fluid}$ 0.9996 and not a volcaniclastic sediment melt component (Fig. 8a). Higher proportions of bulk sediment in the bulk sediment-AMOC mixture would also move mixing curves to intercept some of the samples with lowest $^{143}Nd/^{144}Nd$ and ones with highest $\delta^{41}K$ (Figs. 2, 8a). The volcaniclastic component is too low in $\delta^{41}K$ at a given $^{143}Nd/^{144}Nd$ composition to reproduce the arc lavas (Fig. 8a). Using the larger fractionation factor of $\alpha_{solid\text{-}fluid}$ 0.9985, the volcaniclastic material does reproduce more of the arc lavas, but does fail to reproduce the samples with the lowest $^{143}Nd/^{144}Nd$ (Fig. 8b); potentially even higher fractionation factors are able to reproduce the arc lavas with purely volcaniclastic material, but then will not reproduce the arc lavas in K/La space (Fig. 6b). Using the smaller fractionation factor of $\alpha_{solid\text{-}fluid}$ 0.9998, again the bulk sediment-AMOC material better reproduces the arc lavas but cannot reproduce the arc lavas higher than $\delta^{41}K$−0.35 ‰ (Fig. 8c). Given this and our inferences from Fig. 6, we find that the pure volcaniclastic material is unlikely to be the sediment melt component added to the Mariana arc lava source, and a fraction factor of $\alpha_{solid\text{-}fluid}$ 0.9996 better able to re-create many of the Mariana arc lavas. However experimental data on K isotopic fractionation during slab dehydration is needed to further justify or refute our choice.

Avanzinelli et al. (2012) show based on mixing using $^{206}Pb/^{204}Pb$ and $^{87}Sr/^{86}Sr$ data, that a volcaniclastic sediment partial melt component added to a fluid-fluxed mantle wedge better re-creates the Mariana arc lavas than an average of all subducting lithologies. However, since

the study of Avanzinelli et al. (2012) better approximate partition coefficients for sediment melting are available, e.g., those from Martindale et al. (2013). Following our outlined approach for Nd and $^{143}Nd/^{144}Nd$ modelling, using updated Pb isotopic data from Freymuth et al. (2015), and assuming similar melting behaviour of Ce and Pb during sediment melting ($D^{Ce}_{sediment\text{-}melt} = D^{Pb}_{sediment\text{-}melt}$, a necessary but perhaps not unreasonable assumption given their similar incompatibility during mantle melting) (Tables S3–S7), we find that a bulk sediment-AMOC mix melt added to a fluid fluxed mantle wedge better re-creates more of the Mariana arc lavas than a volcaniclastic melt based on mixing in $^{206}Pb/^{204}Pb$ vs. $^{87}Sr/^{86}Sr$ (Fig. 9), due to a higher Sr partition coefficient than used by Avanzinelli et al. (2012), e.g., from Kessel et al. (2005). The bulk-sediment-AMOC component reproduces more of the Mariana arc lavas than the volcaniclastic component, with up to and just over ~3 % sediment melt addition, similar to our other models (Fig. 9); although a radiogenic Pb sample from Sarigan cannot be reproduced.

Our data also reproduces many of the Izu and Lesser Antilles arc lava samples, and while we have not attempted to model their compositions due to differences in the subducting components between the Mariana, Izu, and Lesser Antilles arcs, it is encouraging that many of the samples can be reproduced with a similar set of processes (Figs. 6 and 8).

In our preferred model for the formation of the Mariana arc lavas from a K isotopic perspective (e.g., Figs. 6a and 8a), serpentinites at the base of a subducting slab dehydrate releasing an oxidising fluid that passes through the overlying oceanic crust leaching fluid mobile elements, with associated isotopic fractionation, gaining necessary elemental and isotopic compositions. This aqueous fluid is delivered to the top of the slab where bulk sediment and AMOC partial melting is induced (Spandler and Pirard, 2013; Klaver et al., 2020; Turner and Langmuir, 2022). The whole package is delivered to the overlying sub-arc mantle wedge as a metasomatic component that modifies the mantle source of the Mariana arc lavas. Results are in agreement with other works that suggest that sediment and AMOC melt in subduction zones (e.g., Freymuth et al., 2019; Klaver et al., 2020; Villalobos-Orchard et al., 2020; Turner and Langmuir, 2022).

5.4. Implications for potassium recycling

Our K results on the Mariana arc lavas are also in line with K systematics from the Izu arc (Parendo et al., 2022b) where a slab released fluid from MORB and sediment is invoked to generate an isotopically heavy K source to explain arc lava systematics. Similar interpretations are applied to the Lesser Antilles arc lavas from K isotopes (Hu et al., 2021a), where isotopically heavier than MORB $\delta^{41}K$ compositions reflect a slab fluid and lighter values the addition of isotopically light sediments. As for the Mariana arc lavas, the compositions of the Lesser Antilles arc lavas also requires the sediment component to be a melt of the bulk subducted sediment (Hu et al., 2021a). These results all indicate that the K isotopic compositions of subducting components can be modified during the dehydration of the slab and release of an aqueous fluid carrying isotopically heavy K and that K isotopes are useful tracers of the addition of sediment components to arc lava sources.

Complementary to the process of arc lava generation, the delivery of isotopically light K, from sediments and subducting slab residues to the mantle represents the potential for K to trace crustal recycling processes. As of yet however, there is no distinguishable K isotopic offset between MORB and OIB sources (Tuller-Ross et al., 2019b) that may be differentially polluted with recycled crustal components; this potentially indicates that the mantle is well mixed in terms of K, or that any heterogeneity is hidden by current analytical precision. Therefore, further work may focus on exploring if any traces of recycled crustal components mix further into the mantle past subduction zones and can be detected in the K isotopic compositions of mantle derived basalts to assess the usefulness of K as a tracer of crustal recycling into the wider mantle.

6. Conclusions

We have presented stable K isotope measurements on a set of well characterised volcanic arc lavas from the Mariana arc, along with a selection of sediment samples from ODP site 801 that represent the subducting sediments at the Mariana trench. The Mariana arc lavas are all isotopically heavier than MORB and form a relatively narrow range in $\delta^{41}K$ (−0.41 to −0.17 ‰) but show positive correlations with tracers of an aqueous fluid released from the dehydration of the subducting slab, e.g., K/La. Heavier K isotopic compositions are associated with this aqueous fluid, in agreement with K isotope systematics on other volcanic arcs, exhumed eclogites and mantle wedge peridotite xenoliths (Liu et al., 2020; Hu et al., 2021a; Parendo et al., 2022b; Wang and Ionov, 2023). Most sediment samples subducting at the Mariana arc have $\delta^{41}K$ within uncertainty of MORB. A notable exception are samples from a thick (~200 m) unit of volcaniclastics that have low $\delta^{41}K$ and influence the $\delta^{41}K$ of the bulk sediment composition at the Mariana arc. Sediment characteristics reflect the removal of isotopically heavy K to the hydrosphere, driving weathered residues to isotopically light values; and marine diagenetic processes, that result in extremely light K isotopic values from the uptake of light K isotopes during the formation authigenic minerals (Hu et al., 2020).

Modelling of isotopically heavy K released in an aqueous fluid from the slab mixed into the Mariana sub-arc mantle with an isotopically light K melt component composed of subducting sediment and AMOC can reproduce the Mariana arc lavas. Our preferred models suggests that the melt component, is a mix of bulk sediment and AMOC, in agreement with other studies (e.g., Freymuth et al., 2015, 2019). Models show that a released aqueous fluid, containing up to 56 % of the K from the subducting slab with $\delta^{41}K$ −0.1 ‰, mixed into the Mariana sub-arc mantle, along with a few percent of the melt component composed of bulk sediment and AMOC is sufficient to create the isotopically heavy K compositions, high K/La ratios, and appropriate $^{143}Nd/^{144}Nd$ compositions of the Mariana arc lavas. Results agree with previously established inter-island variations, where lavas show contributions from an aqueous fluid and variable amounts of sediment addition, that can be traced in $\delta^{41}K$, K/La, and $^{143}Nd/^{144}Nd$. Further work on K isotopic fractionation factors during aqueous fluid release and sediment melting is needed to better constrain our models. This work supports prior evidence that isotopically light K is subducted to the mantle via subducting sediments and residual slabs after subduction zone processing, suggesting the potential for K to trace crustal recycling processes. Whether or not the effects of crustal recycling can be seen in K isotopic systematics of mantle derived basalts remains to be seen.

Data availability

Data are available through Mendeley data at https://doi.org/10.17632/2474843g7x.4.

CRediT authorship contribution statement

Joel B. Rodney: Writing – original draft, Writing – review & editing, Project administration, Methodology, Investigation, Formal analysis, Conceptualization, Funding acquisition. **Théo Tacail:** Writing – review & editing, Methodology. **Jamie Lewis:** Writing – review & editing, Methodology. **Morten B. Andersen:** Writing – review & editing, Validation, Supervision, Project administration, Funding acquisition, Conceptualization. **Tim Elliott:** Writing – review & editing, Validation, Supervision, Project administration, Funding acquisition, Conceptualization.

Declaration of competing interest

The authors declare that they have no known competing financial interests or personal relationships that could have appeared to influence

the work reported in this paper.

Acknowledgements

JBR would like to acknowledge Christopher D. Coath and Carolyn Taylor for the upkeep of the mass spectrometry and clean labs. JBR would like to acknowledge Daniel Stubbs for helpful discussions about geochemical modelling. The authors also acknowledge some helpful comments from Riccardo Avanzinelli. JBR was funded by a NERC GW4 + Doctoral Training Partnership studentship from the Natural Environment Research Council [NE/S007504/1]. JBR, MBA, and TE acknowledge funding from a NERC grant [NE/T012595/1]. JL and TE were also supported by a ERC Adv grant NONUNE 885531. TT was supported by a Marie Curie Sklodowska Postdoctoral Fellowship. We thank Fangzhen Teng for editorial handling and three anonymous reviewers for thorough and constructive reviews that improved the manuscript.

Appendix A. Supplementary material

The supplementary materials for this article have additional details regarding vanadium doping tests to tests the effects on measurements of δ^{41}K (Section 1), and an explanation for modelling the compositions of the Mariana arc lavas (Section 2). The supplementary martials for this article also include seven tables (Tables S1–S7) and two figures (Figs. S1–S2). Table S1 reports the results of the vanadium doping experiments. Table S2 reports our homoscedastic approach for calculating uncertainty of δ^{41}K measurements. Tables S3–S7 reports the inputs used in the modelling of the Mariana arc lava compositions. Fig. S1 shows the results of the vanadium doping experiments. Fig. S2 are additional graphs of Mariana arc lava data with indicators of magmatic differentiation. Supplementary material to this article can be found online at https://doi.org/10.1016/j.gca.2024.07.035.

References

Andersen, M.B., Elliott, T., Freymuth, H., Sims, K.W.W., Niu, Y., Kelley, K.A., 2015. The terrestrial uranium isotope cycle. Nature 517, 356–359.
Avanzinelli, R., Prytulak, J., Skora, S., Heumann, A., Koetsier, G., Elliott, T., 2012. Combined ^{238}U–^{230}Th and ^{235}U–^{231}Pa constraints on the transport of slab-derived material beneath the Mariana Islands. Geochim. Cosmochim. Acta 92, 308–328.
Bevan, D., Coath, C.D., Lewis, J., Schwieters, J., Lloyd, N., Craig, G., Wehrs, H., Elliott, T., 2021. In situ Rb–Sr dating by collision cell, multicollection inductively-coupled plasma mass-spectrometry with pre-cell mass-filter, (CC-MC-ICPMS/MS). J. Anal. At. Spectrom. 36, 917–931.
Bloomer, S.H., Stern, R.J., Smoot, N.C., 1989. Physical volcanology of the submarine Mariana and Volcano Arcs. Bull. Volcanol. 51, 210–224.
Bourg, I.C., Richter, F.M., Christensen, J.N., Sposito, G., 2010. Isotopic mass dependence of metal cation diffusion coefficients in liquid water. Geochim. Cosmochim. Acta 74, 2249–2256.
Brenan, J.M., Shaw, H.F., Phinney, D.L., Ryerson, F.J., 1994. Rutile-aqueous fluid partitioning of Nb, Ta, Hf, Zr, U and Th: implications for high field strength element depletions in island-arc basalts. Earth Planet. Sci. Lett. 128, 327–339.
Carpentier, M., Chauvel, C., Mattielli, N., 2008. Pb–Nd isotopic constraints on sedimentary input into the Lesser Antilles arc system. Earth Planet. Sci. Lett. 272, 199–211.
Chen, Z., Chen, J., Tamehe, L.S., Zhang, Y., Zeng, Z., Xia, X., Cui, Z., Zhang, T., Guo, K., 2022. Heavy copper isotopes in arc-related lavas from cold subduction zones uncover a sub-arc mantle metasomatized by serpentinite-derived sulfate-rich fluids. J. Geophys. Res. Solid Earth 127, e2022JB024910.
Chen, S., Hin, R.C., John, T., Brooker, R., Bryan, B., Niu, Y., Elliott, T., 2019b. Molybdenum systematics of subducted crust record reactive fluid flow from underlying slab serpentine dehydration. Nat. Commun. 10, 4773.
Chen, H., Tian, Z., Tuller-Ross, B., Korotev, R.L., Wang, K., 2019a. High-precision potassium isotopic analysis by MC-ICP-MS: an inter-laboratory comparison and refined K atomic weight. J. Anal. At. Spectrom. 34, 160–171.
Chen, H., Liu, X.-M., Wang, K., 2020. Potassium isotope fractionation during chemical weathering of basalts. Earth Planet. Sci. Lett. 539, 116192.
Chow, T.J., Stern, R.J., Dixon, T.H., 1980. Absolute and relative abundances of K, Rb, Sr and Ba in circum-Pacific island-arc magmas, with special reference to the Marianas. Chem. Geol. 28, 111–121.
Debret, B., Millet, M.-A., Pons, M.-L., Bouilhol, P., Inglis, E., Williams, H., 2016. Isotopic evidence for iron mobility during subduction. Geology 44, 215–218.
Deschamps, F., Godard, M., Guillot, S., Hattori, K., 2013. Geochemistry of subduction zone serpentinites: a review. Lithos 178, 96–127.
Ding, Z.-Y., Liu, S.-K., Su, B.-X., Li, W.-J., Bai, Y., Pan, Q.-Q., Hu, F.-Y., Pang, K.-N., 2023. Potassium isotope fractionation during granite differentiation and implications for crustal K isotope heterogeneity. Lithos 448–449, 107176.
Dixon, T.H., Batiza, R., 1979. Petrology and chemistry of recent lavas in the northern Marianas: implications for the origin of island arc basalts. Contrib. Miner. Petrol. 70, 167–181.
Dixon, J.E., Leist, L., Langmuir, C., Schilling, J.-G., 2002. Recycled dehydrated lithosphere observed in plume-influenced mid-ocean-ridge basalt. Nature 420, 385–389.
Elliott, T., 2003. Tracers of the slab. In: Eiler, J. (Ed.), Inside the Subduction Factory, Geophysical Monograph Series, 138. American Geophysical Union, pp. 23–45.
Elliott, T., Plank, T., Zindler, A., White, W., Bourdon, B., 1997. Element transport from slab to volcanic front at the Mariana arc. J. Geophys. Res. Solid Earth 102, 14991–15019.
Freymuth, H., Vils, F., Willbold, M., Taylor, R.N., Elliott, T., 2015. Molybdenum mobility and isotopic fractionation during subduction at the Mariana arc. Earth Planet. Sci. Lett. 432, 176–186.
Freymuth, H., Ivko, B., Gill, J.B., Tamura, Y., Elliott, T., 2016. Thorium isotope evidence for melting of the mafic oceanic crust beneath the Izu arc. Geochim. Cosmochim. Acta 186, 49–70.
Freymuth, H., Andersen, M.B., Elliott, T., 2019. Uranium isotope fractionation during slab dehydration beneath the Izu arc. Earth Planet. Sci. Lett. 522, 244–254.
Gale, A., Dalton, C.A., Langmuir, C.H., Su, Y., Schilling, J.-G., 2013. The mean composition of ocean ridge basalts. Geochem. Geophys. Geosyst. 14, 489–518.
Hacker, B.R., 2008. H_2O subduction beyond arcs. Geochem. Geophys. Geosyst. 9, Q03001.
Hauff, F., Hoernle, K., Schmidt, A., 2003. Sr-Nd-Pb composition of Mesozoic Pacific oceanic crust (Site 1149 and 801, ODP Leg 185): Implications for alteration of ocean crust and the input into the Izu-Bonin-Mariana subduction system. Geochem. Geophys. Geosyst. 4, 8913.
Hawkesworth, C.J., Gallagher, K., Hergt, J.M., McDermott, F., 1993. Mantle and slab contributions in arc magmas. Annu. Rev. Earth Planet. Sci. 21, 175–204.
Hawthorne, F.C., Calvo, C., 1977. The crystal chemistry of the $M^{+}VO_3$ (M+ = Li, Na, K, NH_4, Tl, Rb, and Cs) pyroxenes. J. Solid State Chem. 22, 157–170.
Hellman, P.L., Smith, R.E., Henderson, P., 1979. The mobility of the rare earth elements: evidence and implications from selected terrains affected by burial metamorphism. Contrib. Miner. Petrol. 71, 23–44.
Hofmann, A.E., Bourg, I.C., DePaolo, D.J., 2012. Ion desolvation as a mechanism for kinetic isotope fractionation in aqueous systems. Proc. Natl. Acad. Sci USA. 109, 18689–18694.
Hole, M.J., Saunders, A.D., Marriner, G.F., Tarney, J., 1984. Subduction of pelagic sediments: implications for the origin of Ce-anomalous basalts from the Mariana Islands. J. Geol. Soc. Lond. 141, 453–472.
Hu, Y., Teng, F.-Z., Plank, T., Chauvel, C., 2020. Potassium isotopic heterogeneity in subducting oceanic plates. Sci. Adv. 6, eabb2472.
Hu, Y., Teng, F.-Z., Chauvel, C., 2021a. Potassium isotopic evidence for sedimentary input to the mantle source of Lesser Antilles lavas. Geochim. Cosmochim. Acta 295, 98–111.
Hu, Y., Teng, F.-Z., Helz, R.T., Chauvel, C., 2021b. Potassium isotope fractionation during magmatic differentiation and the composition of the mantle. J. Geophys. Res. Solid Earth 126, e2020JB021543.
Huang, T.-Y., Teng, F.-Z., Rudnick, R.L., Chen, X.-Y., Hu, Y., Liu, Y.-S., Wu, F.-Y., 2020. Heterogeneous potassium isotopic composition of the upper continental crust. Geochim. Cosmochim. Acta 278, 122–136.
Huang, T.-Y., Teng, F.-Z., Wang, Z.-Z., He, Y.-S., Liu, Z.-C., Wu, F.-Y., 2023. Potassium isotope fractionation during granitic magmatic differentiation: mineral-pair perspectives. Geochim. Cosmochim. Acta 343, 196–211.
Huebner, J.S., Papike, J.J., 1970. Synthesis and crystal chemistry of sodium-potassium richterite, $(Na,K)NaCaMg_5Si_8O_{22}(OH,F)_2$: a model for amphiboles. Am. Mineral. 55, 1973–1992.
Ikeda, Y., Nagao, K., Ishii, T., Matsumoto, D., Stern, R.J., Kagami, H., Arima, M., Bloomer, S.H., 2016. Contributions of slab fluid and sediment melt components to magmatism in the Mariana Arc-Trough system: evidence from geochemical compositions and Sr, Nd, and noble gas isotope systematics. Isl. Arc. 25, 253–273.
Ito, E., Stern, R.J., 1986. Oxygen- and strontium-isotopic investigations of subduction zone volcanism: the case of the Volcano Arc and the Marianas Island Arc. Earth Planet. Sci. Lett. 76, 312–320.
Ito, E., Stern, R.J., Douthitt, C., 2003. Insights into operation of the subduction factory from the oxygen isotopic values of the southern Izu–Bonin–Mariana Arc. Isl. Arc. 12, 383–397.
Jarrard, R.D., 2003. Subduction fluxes of water, carbon dioxide, chlorine, and potassium. Geochem. Geophys. Geosyst. 4, 8905.
John, T., Gussone, N., Podladchikov, Y.Y., Bebout, G.E., Dohmen, R., Halama, R., Klemd, R., Magna, T., Seitz, H.-M., 2012. Volcanic arcs fed by rapid pulsed fluid flow through subducting slabs. Nat. Geosci. 5, 489–492.
Johnson, M.C., Plank, T., 2000. Dehydration and melting experiments constrain the fate of subducted sediments. Geochem. Geophys. Geosyst. 1, 1007.
Karpoff, A.M., 1992. Cenozoic and Mesozoic Sediments from the Pigafetta Basin, Leg 129, Sites 800 and 801: Mineralogical and geochemical trends of the deposits overlying the oldest oceanic crust. Proc. ODP, Sci. Results. 129, 3–30.
Kelley, K.A., Cottrell, E., 2012. The influence of magmatic differentiation on the oxidation state of Fe in a basaltic arc magma. Earth Planet. Sci. Lett. 329–330, 109–121.
Kelley, K.A., Plank, T., Ludden, J., Staudigel, H., 2003. Composition of altered oceanic crust at ODP Sites 801 and 1149. Geochem. Geophys. Geosyst. 4, 8910.

Kelley, K.A., Plank, T., Newman, S., Stolper, E.M., Grove, T.L., Parman, S., Hauri, E.H., 2010. Mantle melting as a function of water content beneath the Mariana Arc. J. Petrol. 51, 1711–1738.
Kessel, R., Schmidt, M.W., Ulmer, P., Pettke, T., 2005. Trace element signature of subduction-zone fluids, melts and supercritical liquids at 120–180 km depth. Nature 437, 724–727.
Klaver, M., Lewis, J., Parkinson, I.J., Elburg, M.A., Vroon, P.Z., Kelley, K.A., Elliott, T., 2020. Sr isotopes in arcs revisited: tracking slab dehydration using $\delta^{88/86}$Sr and ^{87}Sr/^{86}Sr systematics of arc lavas. Geochim. Cosmochim. Acta 288, 101–119.
König, S., Wille, M., Voegelin, A., Schoenberg, R., 2016. Molybdenum isotope systematics in subduction zones. Earth Planet. Sci. Lett. 447, 95–102.
Kuhnel, W.W., Jacobsen, S.B., Li, Y., Ku, Y., Petaev, M.I., Huang, S., Wu, Z., Wang, K., 2021. High-temperature inter-mineral potassium isotope fractionation: implications for K-Ca–Ar chronology. ACS Earth Space Chem. 5, 2740–2754.
Lancelot, Y., Larson, R.L., Fisher, A., Abrams, L., Rabinowitz, P.D., Meyer, A.W., Garrison, L.E., 1990. Ocean Drilling Program, Leg 129 Preliminary Report: Old Pacific Crust. Program, Texas A & M University.
Lewis, J., Luu, T.-H., Coath, C.D., Wehrs, H., Schwieters, J.B., Elliott, T., 2022. Collision course; high-precision mass-independent and mass-dependent calcium isotope measurements using the prototype collision cell MC-ICPMS/MS, Proteus. Chem. Geol. 614, 121185.
Li, W., Beard, B.L., Li, S., 2016. Precise measurement of stable potassium isotope ratios using a single focusing collision cell multi-collector ICP-MS. J. Anal. At. Spectrom. 31, 1023–1029.
Li, S., Li, W., Beard, B.L., Raymo, M.E., Wang, X., Chen, Y., Chen, J., 2019a. K isotopes as a tracer for continental weathering and geological K cycling. Proc. Natl. Acad. Sci. 116, 8740–8745.
Li, W., Liu, X.-M., Wang, K., McManus, J., Haley, B.A., Takahashi, Y., Shakouri, M., Hu, Y., 2022. Potassium isotope signatures in modern marine sediments: Insights into early diagenesis. Earth Planet. Sci. Lett. 599, 117849.
Li, Y., Wang, W., Wu, Z., Huang, S., 2019b. First-principles investigation of equilibrium K isotope fractionation among K-bearing minerals. Geochim. Cosmochim. Acta 264, 30–42.
Liu, H., Xiao, Y., van den Kerkhof, A., Wang, Y., Zeng, L., Guo, H., 2019. Metamorphism and fluid evolution of the Sumdo eclogite, Tibet: constraints from mineral chemistry, fluid inclusions and oxygen isotopes. J. Asian Earth Sci. 172, 292–307.
Liu, H., Wang, K., Sun, W.-D., Xiao, Y., Xue, Y.-Y., Tuller-Ross, B., 2020. Extremely light K in subducted low-T altered oceanic crust: implications for K recycling in subduction zone. Geochim. Cosmochim. Acta 277, 206–223.
Marschall, H.R., Schumacher, J.C., 2012. Arc magmas sourced from mélange diapirs in subduction zones. Nat. Geosci. 5, 862–867.
Marske, J.P., Pietruszka, A.J., Trusdell, F.A., Garcia, M.O., 2011. Geochemistry of southern Pagan Island lavas, Mariana arc: the role of subduction zone processes. Contrib. Miner. Petrol. 162, 231–252.
Martindale, M., Skora, S., Pickles, J., Elliott, T., Blundy, J., Avanzinelli, R., 2013. High pressure phase relations of subducted volcaniclastic sediments from the west pacific and their implications for the geochemistry of Mariana arc magmas. Chem. Geol. 342, 94–109.
Maunder, B.L., Kendrick, M.A., Ribeiro, J.M., Nebel, O., 2024. A negligible role for forearc serpentinites and mélange diapirism in contributing halogens to Mariana arc magmas. Earth Planet. Sci. Lett. 625, 118498.
Mazza, S.E., Stracke, A., Gill, J.B., Kimura, J.-I., Kleine, T., 2020. Tracing dehydration and melting of the subducted slab with tungsten isotopes in arc lavas. Earth Planet. Sci. Lett. 530, 115942.
Meijer, A., 1976. Pb and Sr isotopic data bearing on the origin of volcanic rocks from the Mariana island-arc system. GSA Bull. 87, 1358–1369.
Meijer, A., Reagan, M., 1981. Petrology and geochemistry of the island of Sarigan in the Mariana arc; calc-alkaline volcanism in an oceanic setting. Contrib. Miner. Petrol. 77, 337–354.
Meijer, A., Reagan, M., Ellis, H., Shafiqullah, M., Sutter, J., Damon, P., Kling, S., 1983. Chronology of volcanic events in the Eastern Philippine Sea. In: Hayes, D.E. (Ed.), The Tectonic and Geologic Evolution of Southeast Asian Seas and Islands: Part 2, Geophysical Monograph Series, 27. American Geophysical Union, pp. 349–359.
Morgan, L.E., Ramos, D.P.S., Davidheiser-Kroll, B., Faithfull, J., Lloyd, N.S., Ellam, R.M., Higgins, J.A., 2018. High-precision ^{41}K/^{39}K measurements by MC-ICP-MS indicate terrestrial variability of δ^{41}K. J. Anal. At. Spectrom. 33, 175–186.
Moynier, F., Hu, Y., Dai, W., Kubik, E., Mahan, B., Moureau, J., 2021. Potassium isotopic composition of seven widely available biological standards using collision cell (CC)-MC-ICP-MS. J. Anal. At. Spectrom. 36, 2444–2448.
Nielsen, S.G., Marschall, H.R., 2017. Geochemical evidence for mélange melting in global arcs. Sci. Adv. 3, e1602402.
Nielsen, S.G., Shu, Y., Auro, M., Yogodzinski, G., Shinjo, R., Plank, T., Kay, S.M., Horner, T.J., 2020. Barium isotope systematics of subduction zones. Geochim. Cosmochim. Acta 275, 1–18.
Pallister, J.S., Trusdell, F.A., Brownfield, I.K., Siems, D.F., Budahn, J.R., Sutley, S.F., 2005. The 2003 phreatomagmatic eruptions of Anatahan volcano - textural and petrologic features of deposits at an emergent island volcano. J. Volcanol. Geoth. Res. 146, 208–225.
Parendo, C.A., Jacobsen, S.B., Plank, T., 2022a. Potassium-isotope variations of marine sediments adjacent to the Izu-Bonin Trench and Nankai Trough. Geochim. Cosmochim. Acta 337, 166–181.
Parendo, C.A., Jacobsen, S.B., Kimura, J.-I., Taylor, R.N., 2022b. Across-arc variations in K-isotope ratios in lavas of the Izu arc: evidence for progressive depletion of the slab in K and similarly mobile elements. Earth Planet. Sci. Lett. 578, 117291.
Peacock, S.M., 2001. Are the lower planes of double seismic zones caused by serpentine dehydration in subducting oceanic mantle? Geology 29, 299–302.
Pearce, J., 1983. Role of the sub-continental lithosphere in magma genesis at active continental margin. In: Hawkesworth, C.J., Norry, M. (Eds.), Continental Basalts and Mantle Xenoliths. Shiva Publications, pp. 230–249.
Pearce, J.A., Kempton, P.D., Nowell, G.M., Noble, S.R., 1999. Hf-Nd element and isotope perspective on the nature and provenance of mantle and subduction components in Western Pacific Arc-Basin systems. J. Petrol. 40, 1579–1611.
Pearce, J.A., Stern, R.J., Bloomer, S.H., Fryer, P., 2005. Geochemical mapping of the Mariana arc-basin system: implications for the nature and distribution of subduction components. Geochem. Geophys. Geosyst. 6, Q07006.
Plank, T., 2005. Constraints from thorium/lanthanum on sediment recycling at subduction zones and the evolution of the continents. J. Petrol. 46, 921–944.
Plank, T., 2014. 4.17 - The chemical composition of subducting sediments. In: Holland, H.D., Turekian, K.K. (Eds.), Treatise on Geochemistry, second edition. Elsevier, pp. 607–629.
Plank, T., Langmuir, C.H., 1993. Tracing trace elements from sediment input to volcanic output at subduction zones. Nature 362, 739–743.
Plank, T., Langmuir, C.H., 1998. The chemical composition of subducting sediment and its consequences for the crust and mantle. Chem. Geol. 145, 325–394.
Pons, M.-L., Debret, B., Bouilhol, P., Delacour, A., Williams, H., 2016. Zinc isotope evidence for sulfate-rich fluid transfer across subduction zones. Nat. Commun. 7, 13794.
Prytulak, J., Nielsen, S.G., Plank, T., Barker, M., Elliott, T., 2013. Assessing the utility of thallium and thallium isotopes for tracing subduction zone inputs to the Mariana arc. Chem. Geol. 345, 139–149.
Robinson, J.A.C., Wood, B.J., Blundy, J.D., 1998. The beginning of melting of fertile and depleted peridotite at 1.5 GPa. Earth Planet. Sci. Lett. 155, 97–111.
Salimullah, A.R.M., Stow, D.A.V., 1992. Wireline log signatures of resedimented volcaniclastic facies, ODP Leg 129, West Central Pacific. Geol. Soc. Lond. Spec. Publ. 65, 87–97.
Salters, V.J.M., Stracke, A., 2004. Composition of the depleted mantle. Geochem. Geophys. Geosyst. 5, Q05B07.
Santiago Ramos, D.P., Morgan, L.E., Lloyd, N.S., Higgins, J.A., 2018. Reverse weathering in marine sediments and the geochemical cycle of potassium in seawater: Insights from the K isotopic composition (^{41}K/^{39}K) of deep-sea pore-fluids. Geochim. Cosmochim. Acta 236, 99–120.
Santiago Ramos, D.P., Coogan, L.A., Murphy, J.G., Higgins, J.A., 2020. Low-temperature oceanic crust alteration and the isotopic budgets of potassium and magnesium in seawater. Earth Planet. Sci. Lett. 541, 116290.
Schauble, E.A., 2004. Applying stable isotope fractionation theory to new systems. Rev. Mineral. Geochem. 55, 65–111.
Schmidt, M.W., Poli, S., 1998. Experimentally based water budgets for dehydrating slabs and consequences for arc magma generation. Earth Planet. Sci. Lett. 163, 361–379.
Schmidt, M.W., Vielzeuf, D., Auzanneau, E., 2004. Melting and dissolution of subducting crust at high pressures: the key role of white mica. Earth Planet. Sci. Lett. 228, 65–84.
Seno, T., 1977. The instantaneous rotation vector of the Philippine sea plate relative to the Eurasian plate. Tectonophysics 42, 209–226.
Skora, S., Blundy, J., 2010. High-pressure hydrous phase relations of radiolarian clay and implications for the involvement of subducted sediment in arc magmatism. J. Petrol. 51, 2211–2243.
Spandler, C., Pirard, C., 2013. Element recycling from subducting slabs to arc crust: a review. Lithos 170–171, 208–223.
Spandler, C., Mavrogenes, J., Hermann, J., 2007. Experimental constraints on element mobility from subducted sediments using high-P synthetic fluid/melt inclusions. Chem. Geol. 239, 228–249.
Spandler, C., Pettke, T., Rubatto, D., 2011. Internal and external fluid sources for eclogite-facies veins in the Monviso Meta-ophiolite, Western Alps: implications for fluid flow in subduction zones. J. Petrol. 52, 1207–1236.
Stern, R.J., 1979. On the origin of andesite in the northern Mariana Island Arc: implications from Agrigan. Contrib. Miner. Petrol. 68, 207–219.
Stern, R.J., Fouch, M.J., Klemperer, S.L., 2003. An overview of the Izu-Bonin-Mariana subduction factory. In: Eiler, J. (Ed.), Inside the Subduction Factory, Geophysical Monograph Series, 138. American Geophysical Union, pp. 175–222.
Stern, R.J., Ito, E., 1983. Trace-element and isotopic constraints on the source of magmas in the active volcano and Mariana island arcs, Western Pacific. J. Volcanol. Geotherm. Res. 18, 461–482.
Stern, R.J., Kohut, E., Bloomer, S.H., Leybourne, M., Fouch, M., Vervoort, J., 2006. Subduction factory processes beneath the Guguan cross-chain, Mariana Arc: no role for sediments, are serpentinites important? Contrib. Miner. Petrol. 151, 202–221.
Stracke, A., 2012. Earth's heterogeneous mantle: a product of convection-driven interaction between crust and mantle. Chem. Geol. 330–331, 274–299.
Stubbs, D., Yang, R., Coath, C.D., John, T., Elliott, T., 2022. Tungsten isotopic fractionation at the Mariana arc and constraints on the redox conditions of subduction zone fluids. Geochim. Cosmochim. Acta 334, 135–154.
Tacail, T., Lewis, J., Clauss, M., Coath, C.D., Evershed, R., Albalat, E., Elliott, T.E., Tütken, T., 2023. Diet, cellular and systemic homeostasis control the cycling of potassium stable isotopes in endothermic vertebrates. Metallomics: Integr. Biometal Sci. 15, mfad065.
Tamura, Y., Ishizuka, O., Stern, R.J., Nichols, A.R.L., Kawabata, H., Hirahara, Y., Chang, Q., Miyazaki, T., Kimura, J.-I., Embley, R.W., Tatsumi, Y., 2014. Mission immiscible: distinct subduction components generate two primary magmas at Pagan Volcano, Mariana Arc. J. Petrol. 55, 63–101.
Teng, F.-Z., Hu, Y., Ma, J.-L., Wei, G.-J., Rudnick, R.L., 2020. Potassium isotope fractionation during continental weathering and implications for global K isotopic balance. Geochim. Cosmochim. Acta 278, 261–271.

Tollstrup, D.L., Gill, J.B., 2005. Hafnium systematics of the Mariana arc: evidence for sediment melt and residual phases. Geology 33, 737–740.
Tuller-Ross, B., Savage, P.S., Chen, H., Wang, K., 2019a. Potassium isotope fractionation during magmatic differentiation of basalt to rhyolite. Chem. Geol. 525, 37–45.
Tuller-Ross, B., Marty, B., Chen, H., Kelley, K.A., Lee, H., Wang, K., 2019b. Potassium isotope systematics of oceanic basalts. Geochim. Cosmochim. Acta 259, 144–154.
Turner, S.J., Langmuir, C.H., 2022. Sediment and ocean crust both melt at subduction zones. Earth Planet. Sci. Lett. 584, 117424.
Ulmer, P., Trommsdorff, V., 1995. Serpentine stability to mantle depths and subduction-related magmatism. Science 268, 858–861.
van Keken, P.E., Hacker, B.R., Syracuse, E.M., Abers, G.A., 2011. Subduction factory: 4. Depth-dependent flux of H_2O from subducting slabs worldwide. J. Geophys. Res. Solid Earth. 116, B01401.
Vervoort, J.D., Plank, T., Prytulak, J., 2011. The Hf–Nd isotopic composition of marine sediments. Geochim. Cosmochim. Acta 75, 5903–5926.
Villalobos-Orchard, J., Freymuth, H., O'Driscoll, B., Elliott, T., Williams, H., Casalini, M., Willbold, M., 2020. Molybdenum isotope ratios in Izu arc basalts: the control of subduction zone fluids on compositional variations in arc volcanic systems. Geochim. Cosmochim. Acta 288, 68–82.
von Huene, R.E., Scholl, D.W., 1991. Observations at convergent margins concerning sediment subduction, subduction erosion, and the growth of continental crust. Rev. Geophys. 29, 279–316.
Wade, J.A., Plank, T., Stern, R.J., Tollstrup, D.L., Gill, J.B., O'Leary, J.C., Eiler, J.M., Moore, R.B., Woodhead, J.D., Trusdell, F., Fischer, T.P., Hilton, D.R., 2005. The May 2003 eruption of Anatahan volcano, Mariana Islands: Geochemical evolution of a silicic island-arc volcano. J. Volcanol. Geoth. Res. 146, 139–170.
Wang, K., Close, H.G., Tuller-Ross, B., Chen, H., 2020. Global average potassium isotope composition of modern seawater. ACS Earth Space Chem. 4, 1010–1017.
Wang, K., Ionov, D.A., 2023. Potassium isotope evidence for slab-derived fluids in the sub-arc mantle. Earth Planet. Sci. Lett. 619, 118315.
Wang, K., Jacobsen, S.B., 2016. An estimate of the Bulk Silicate Earth potassium isotopic composition based on MC-ICPMS measurements of basalts. Geochim. Cosmochim. Acta 178, 223–232.
Wang, K., Li, W., Li, S., Tian, Z., Koefoed, P., Zheng, X.-Y., 2021. Geochemistry and cosmochemistry of potassium stable isotopes. Geochemistry 81, 125786.
Wang, Z.-Z., Teng, F.-Z., Wu, F.-Y., Liu, Z.-C., Liu, X.-C., Liu, S.-A., Huang, T.-Y., 2022. Extensive crystal fractionation of high-silica magmas revealed by K isotopes. Sci. Adv. 8, eabo4492.
White, W.M., Klein, E.M., 2014. 4.13 - Composition of the oceanic crust. In: Holland, H. D., Turekian, K.K. (Eds.), Treatise on Geochemistry, second edition. Elsevier, pp. 457–496.
White, W.M., Patchett, J., 1984. Hf Nd Sr isotopes and incompatible element abundances in island arcs: implications for magma origins and crust-mantle evolution. Earth Planet. Sci. Lett. 67, 167–185.
Williams, H.M., Prytulak, J., Woodhead, J.D., Kelley, K.A., Brounce, M., Plank, T., 2018. Interplay of crystal fractionation, sulfide saturation and oxygen fugacity on the iron isotope composition of arc lavas: an example from the Marianas. Geochim. Cosmochim. Acta 226, 224–243.
Woodhead, J.D., 1988. The origin of geochemical variations in Mariana Lavas: a general model for petrogenesis in intra-oceanic island arcs? J. Petrol. 29, 805–830.
Woodhead, J.D., 1989. Geochemistry of the Mariana arc (western Pacific): source composition and processes. Chem. Geol. 76, 1–24.
Woodhead, J., Eggins, S., Gamble, J., 1993. High field strength and transition element systematics in island arc and back-arc basin basalts: evidence for multi-phase melt extraction and a depleted mantle wedge. Earth Planet. Sci. Lett. 114, 491–504.
Woodhead, J.D., Fraser, D.G., 1985. Pb, Sr and ^{10}Be isotopic studies of volcanic rocks from the Northern Mariana Islands implications for magma genesis and crustal recycling in the Western Pacific. Geochim. Cosmochim. Acta 49, 1925–1930.
Woodhead, J., Hergt, J., Greig, A., Edwards, L., 2011. Subduction zone Hf-anomalies: mantle messenger, melting artefact or crustal process? Earth Planet. Sci. Lett. 304, 231–239.
Woodhead, J., Stern, R.J., Pearce, J., Hergt, J., Vervoort, J., 2012. Hf-Nd isotope variation in Mariana Trough basalts: the importance of "ambient mantle" in the interpretation of subduction zone magmas. Geology 40, 539–542.
Wu, F., Qi, Y., Yu, H., Tian, S., Hou, Z., Huang, F., 2016. Vanadium isotope measurement by MC-ICP-MS. Chem. Geol. 421, 17–25.
Wu, F., Turner, S., Schaefer, B.F., 2020. Mélange versus fluid and melt enrichment of subarc mantle: a novel test using barium isotopes in the Tonga-Kermadec arc. Geology 48, 1053–1057.
Zack, T., John, T., 2007. An evaluation of reactive fluid flow and trace element mobility in subducting slabs. Chem. Geol. 239, 199–216.
Zack, T., Rivers, T., Foley, S., 2001. Cs–Rb–Ba systematics in phengite and amphibole: an assessment of fluid mobility at 2.0 GPa in eclogites from Trescolmen, Central Alps. Contrib. Mineral. Petrol. 140, 651–669.
Zeng, H., Rozsa, V.F., Nie, N.X., Zhang, Z., Pham, T.A., Galli, G., Dauphas, N., 2019. Ab initio calculation of equilibrium isotopic fractionations of potassium and rubidium in minerals and water. ACS Earth Space Chem. 3, 2601–2612.